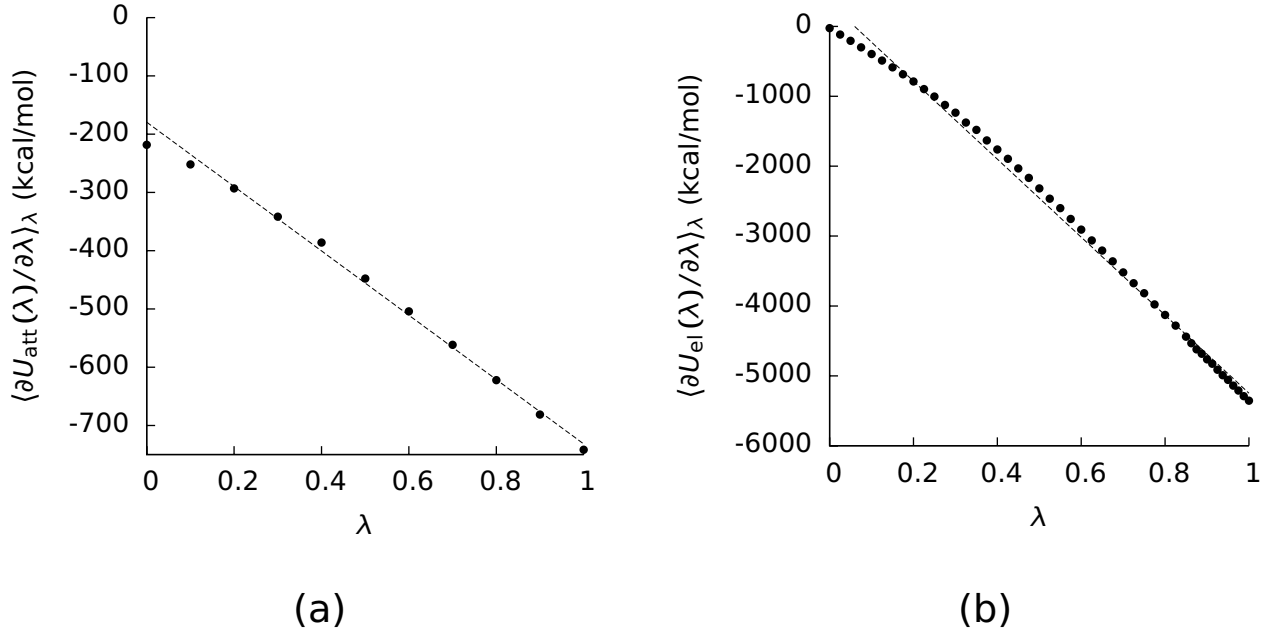

Figure 1: a) The derivative ($\langle \partial U_{\rm att}/\partial\lambda \rangle_\lambda$) of the λ-dependent potential used to compute the attractive component ($\Delta G_{\rm att}$) of the Lennard-Jones cavity insertion energy ($\Delta G_{\rm vdw}$) as a function of the intergration coordinate (λ), averaged over an ensemble where the interaction energy between an atom i in the solute and an atom j in the solvent was given by the λ-dependent potential ($U^{ij}_{\rm att}(\lambda)$), as defined in the Methods, for the 1BRS barnase-barstar complex. b) The derivative ($\langle \partial U_{\rm el}/\partial\lambda \rangle_\lambda$) of the λ-dependent potential used to compute the electrostatic component ($\Delta G_{\rm el}$) of the solvation free energy (ΔG) as a function of the intergration coordinate (λ), averaged over an ensemble where the interaction energy between an atom i in the solute and an atom j in the solvent was given by the λ-dependent potential ($U^{ij}_{\rm el}(\lambda)$), as defined in the Methods, for the 1BRS barnase-barstar complex. The dotted lines are least-squares lines drawn through the data. The squares (R^2) of the Pearson correlation coefficients are a) 0.994 and b) 0.995.

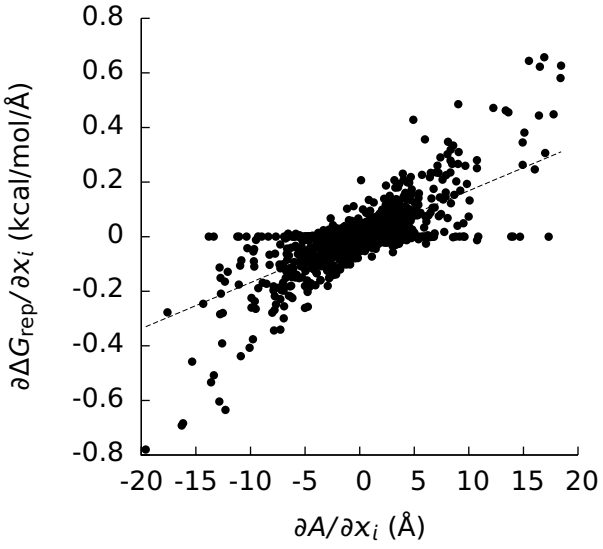
0.8
0.6
0.4
0.2
0
-0.2
-0.4
-0.6
-0.8
-20 -15 -10 -5 0 5 10 15 20
$\partial\Delta G_{rep}/\partial x_i$ (kcal/mol/Å)
$\partial A/\partial x_i$ (Å)

(a)

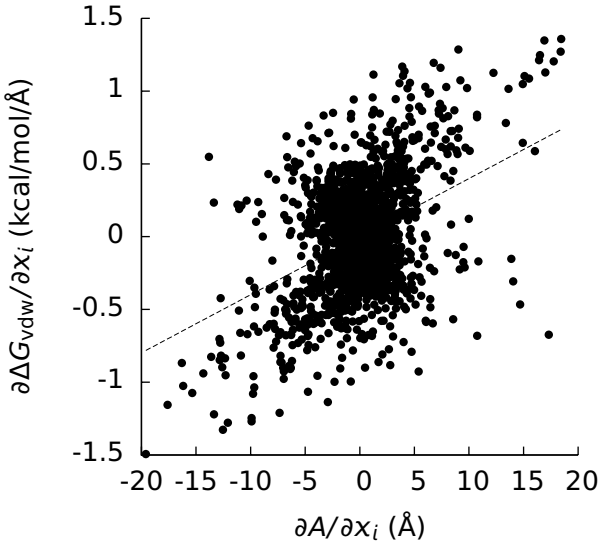
1.5
1
0.5
0
-0.5
-1
-1.5
-20 -15 -10 -5 0 5 10 15 20
$\partial\Delta G_{vdw}/\partial x_i$ (kcal/mol/Å)
$\partial A/\partial x_i$ (Å)

(b)

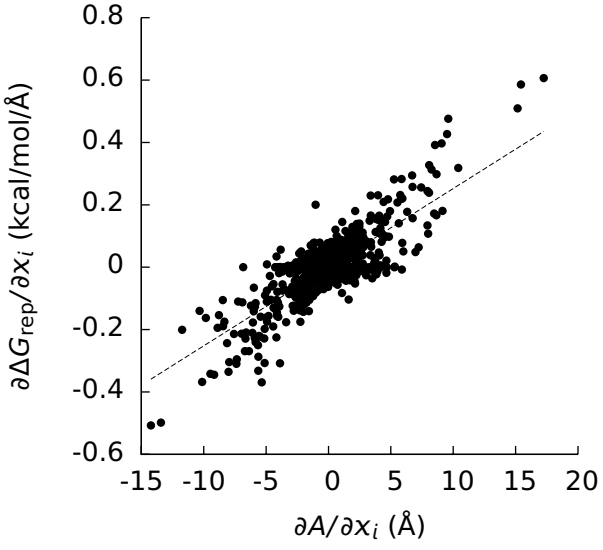
0.8
0.6
0.4
0.2
0
-0.2
-0.4
-0.6
-15 -10 -5 0 5 10 15 20
$\partial\Delta G_{rep}/\partial x_i$ (kcal/mol/Å)
$\partial A/\partial x_i$ (Å)

(c)

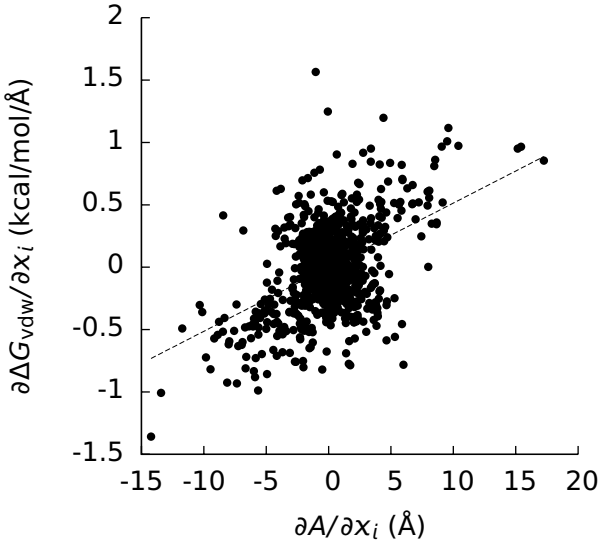
2
1.5
1
0.5
0
-0.5
-1
-1.5
-15 -10 -5 0 5 10 15 20
$\partial\Delta G_{vdw}/\partial x_i$ (kcal/mol/Å)
$\partial A/\partial x_i$ (Å)

(d)

Figure 2: a) The derivative ($\partial \Delta G_{\mathrm{rep}} / \partial x_i$) of the repulsive component (ΔG_{rep}) of the Lennard-Jones cavity insertion free energy (ΔG_{vdw}) with respect to the coordinates (x_i) of the atomic centers versus the derivative ($\partial A / \partial x_i$) of the solvent-accessible area (A) with respect to x_i for the first component of the 1ACB complex. b) $\partial \Delta G_{\mathrm{vdw}} / \partial x_i$ versus $\partial A / \partial x_i$ for the first component of the 1ACB complex. c) $\partial \Delta G_{\mathrm{rep}} / \partial x_i$ versus $\partial A / \partial x_i$ for the second component of the 1ACB complex. d) $\partial \Delta G_{\mathrm{vdw}} / \partial x_i$ versus $\partial A / \partial x_i$ for the second component of the 1ACB complex. The dotted lines are least-squares lines drawn through the data. The slopes and squares of the Pearson correlation coefficients of these lines can be found in Table 1 of the main text.

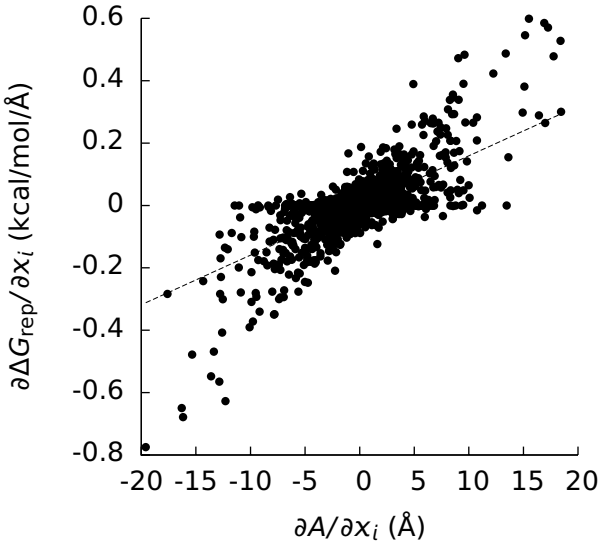
0.6
0.4
0.2
0
-0.2
-0.4
-0.6
-0.8
-20 -15 -10 -5 0 5 10 15 20
$\partial\Delta G_{\mathrm{rep}}/\partial x_i$ (kcal/mol/Å)
$\partial A/\partial x_i$ (Å)

(a)

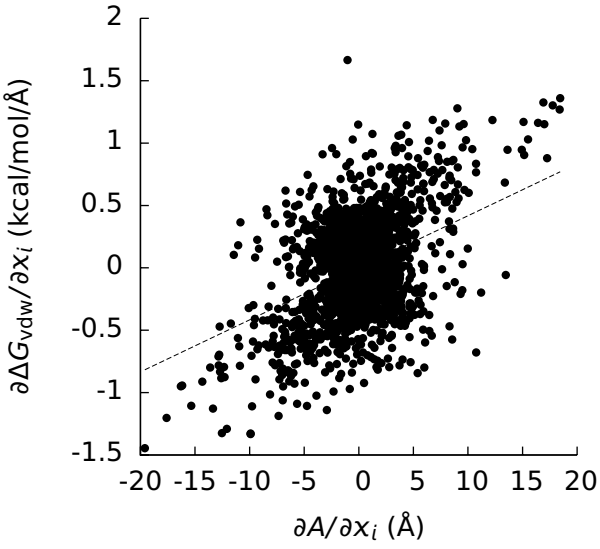
2
1.5
1
0.5
0
-0.5
-1
-1.5
-20 -15 -10 -5 0 5 10 15 20
$\partial\Delta G_{\mathrm{vdw}}/\partial x_i$ (kcal/mol/Å)
$\partial A/\partial x_i$ (Å)

(b)

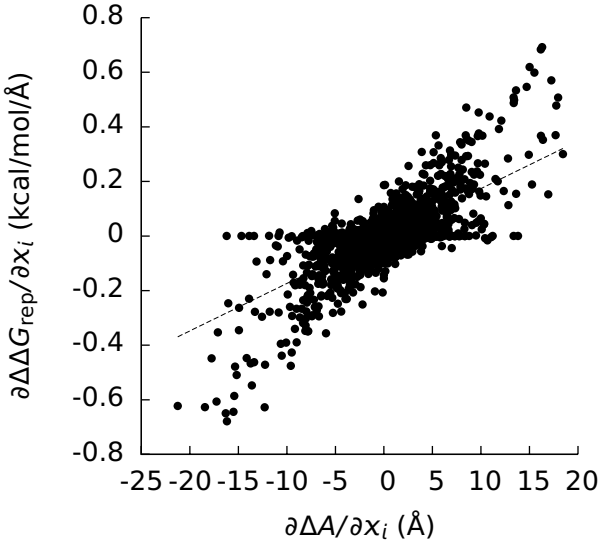
0.8
0.6
0.4
0.2
0
-0.2
-0.4
-0.6
-0.8
-25 -20 -15 -10 -5 0 5 10 15 20
$\partial\Delta\Delta G_{\mathrm{rep}}/\partial x_i$ (kcal/mol/Å)
$\partial\Delta A/\partial x_i$ (Å)

(c)

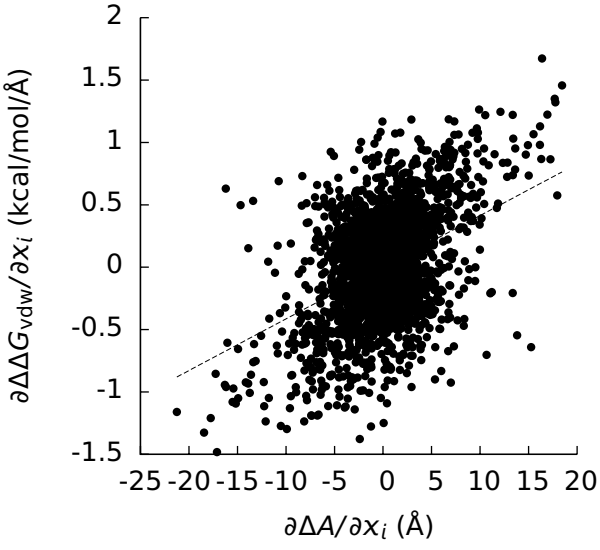
2
1.5
1
0.5
0
-0.5
-1
-1.5
-25 -20 -15 -10 -5 0 5 10 15 20
$\partial\Delta\Delta G_{\mathrm{vdw}}/\partial x_i$ (kcal/mol/Å)
$\partial\Delta A/\partial x_i$ (Å)

(d)

Figure 3: a) The derivative ($\partial \Delta G_{\mathrm{rep}} / \partial x_i$) of the repulsive component (ΔG_{rep}) of the Lennard-Jones cavity insertion free energy (ΔG_{vdw}) with respect to the coordinates (x_i) of the atomic centers versus the derivative ($\partial A / \partial x_i$) of the solvent-accessible area (A) with respect to x_i for the 1ACB complex. b) $\partial \Delta G_{\mathrm{vdw}} / \partial x_i$ versus $\partial A / \partial x_i$ for the 1ACB complex. c) The derivative ($\partial \Delta \Delta G_{\mathrm{rep}} / \partial x_i$) of the repulsive component ($\Delta \Delta G_{\mathrm{rep}}$) of the Lennard-Jones component ($\Delta \Delta G_{\mathrm{vdw}}$) of the binding free energy with respect to x_i versus the derivative ($\partial \Delta A / \partial x_i$) of the change ($\Delta A$) in A upon binding with respect to x_i for the 1ACB complex. d) $\partial \Delta \Delta G_{\mathrm{vdw}} / \partial x_i$ versus $\partial \Delta A / \partial x_i$ for the 1ACB complex. The dotted lines are least-squares lines drawn through the data. The slopes and squares of the Pearson correlation coefficients of these lines can be found in Table 1 of the main text.

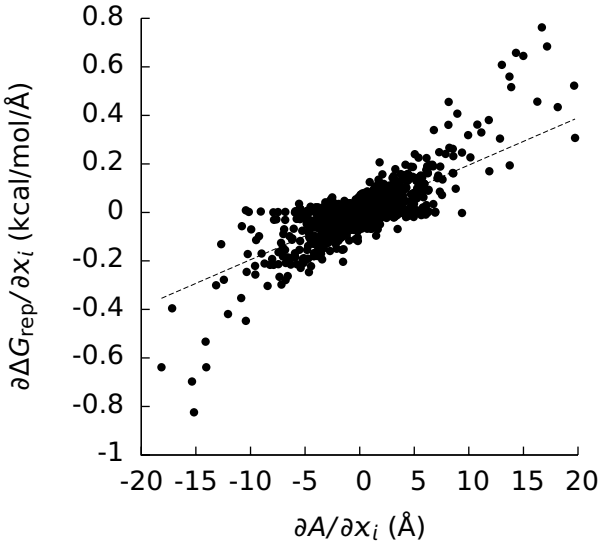
0.8
0.6
0.4
0.2
0
-0.2
-0.4
-0.6
-0.8
-1
-20 -15 -10 -5 0 5 10 15 20
∂ΔG_rep/∂x_i (kcal/mol/Å)
∂A/∂x_i (Å)

(a)

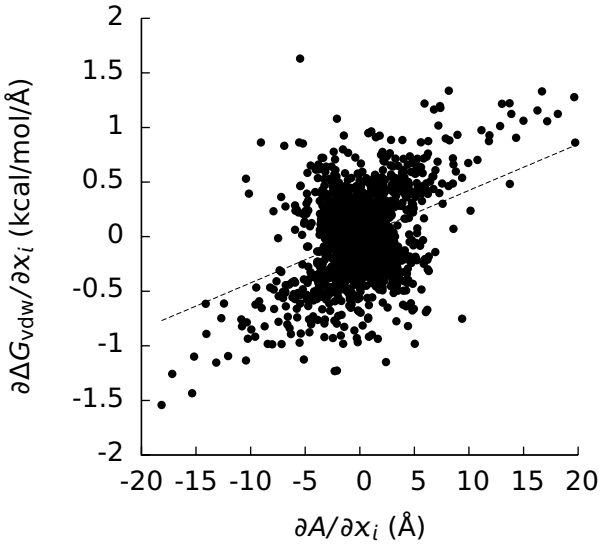
2
1.5
1
0.5
0
-0.5
-1
-1.5
-2
-20 -15 -10 -5 0 5 10 15 20
∂ΔG_vdw/∂x_i (kcal/mol/Å)
∂A/∂x_i (Å)

(b)

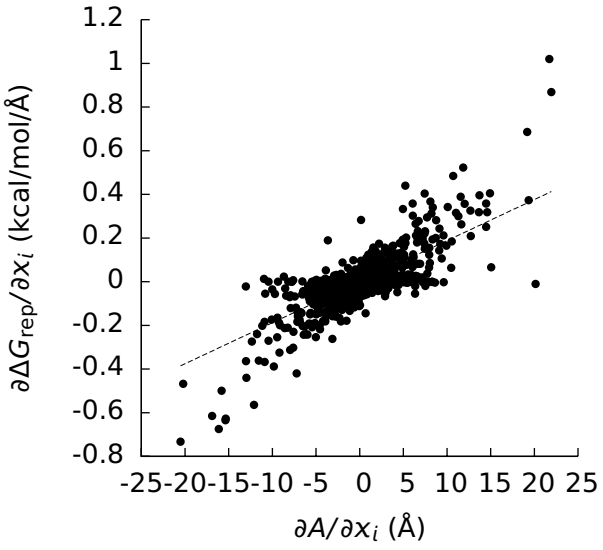
1.2
1
0.8
0.6
0.4
0.2
0
-0.2
-0.4
-0.6
-0.8
-25-20-15-10 -5 0 5 10 15 20 25
∂ΔG_rep/∂x_i (kcal/mol/Å)
∂A/∂x_i (Å)

(c)

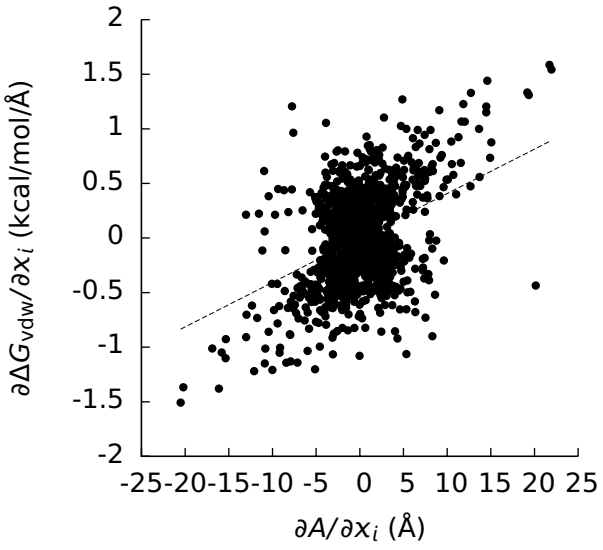
2
1.5
1
0.5
0
-0.5
-1
-1.5
-2
-25-20-15-10 -5 0 5 10 15 20 25
∂ΔG_vdw/∂x_i (kcal/mol/Å)
∂A/∂x_i (Å)

(d)

Figure 4: a) The derivative ($\partial \Delta G_{\mathrm{rep}} / \partial x_i$) of the repulsive component (ΔG_{rep}) of the Lennard-Jones cavity insertion free energy (ΔG_{vdw}) with respect to the coordinates (x_i) of the atomic centers versus the derivative ($\partial A / \partial x_i$) of the solvent-accessible area (A) with respect to x_i for the first component of the 1AVX complex. b) $\partial \Delta G_{\mathrm{vdw}} / \partial x_i$ versus $\partial A / \partial x_i$ for the first component of the 1AVX complex. c) $\partial \Delta G_{\mathrm{rep}} / \partial x_i$ versus $\partial A / \partial x_i$ for the second component of the 1AVX complex. d) $\partial \Delta G_{\mathrm{vdw}} / \partial x_i$ versus $\partial A / \partial x_i$ for the second component of the 1AVX complex. The dotted lines are least-squares lines drawn through the data. The slopes and squares of the Pearson correlation coefficients of these lines can be found in Table 1 of the main text.

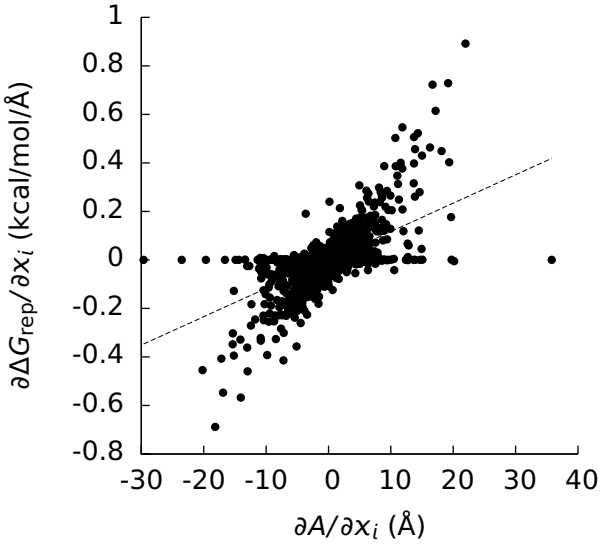
1
0.8
0.6
0.4
0.2
0
-0.2
-0.4
-0.6
-0.8
-30 -20 -10 0 10 20 30 40
$\partial\Delta G_{rep}/\partial x_i$ (kcal/mol/Å)
$\partial A/\partial x_i$ (Å)

(a)

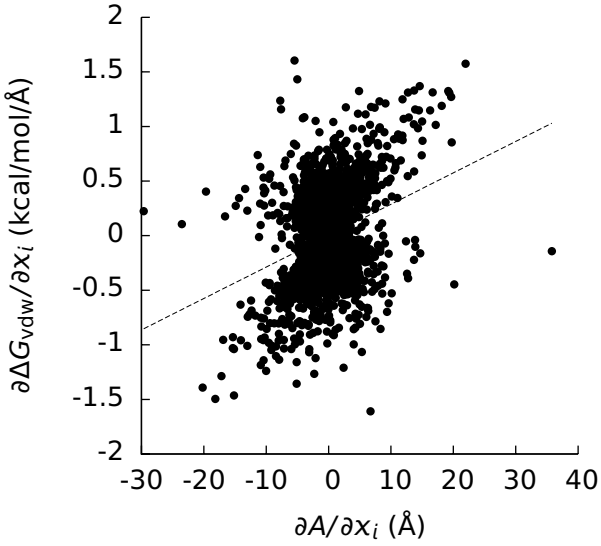
2
1.5
1
0.5
0
-0.5
-1
-1.5
-2
-30 -20 -10 0 10 20 30 40
$\partial\Delta G_{vdw}/\partial x_i$ (kcal/mol/Å)
$\partial A/\partial x_i$ (Å)

(b)

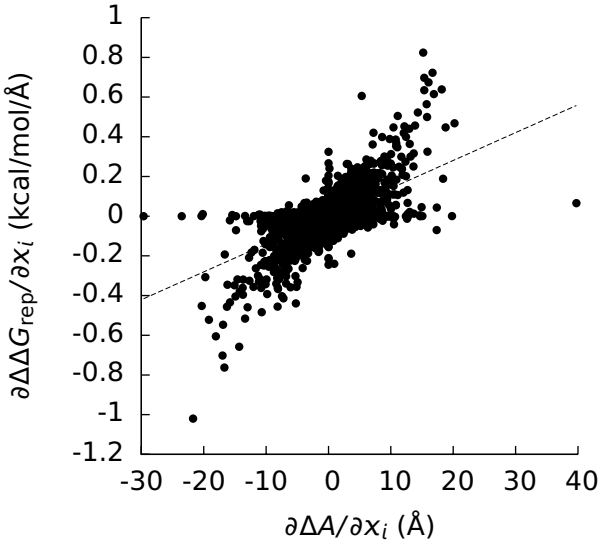
1
0.8
0.6
0.4
0.2
0
-0.2
-0.4
-0.6
-0.8
-1
-1.2
-30 -20 -10 0 10 20 30 40
$\partial\Delta\Delta G_{rep}/\partial x_i$ (kcal/mol/Å)
$\partial\Delta A/\partial x_i$ (Å)

(c)

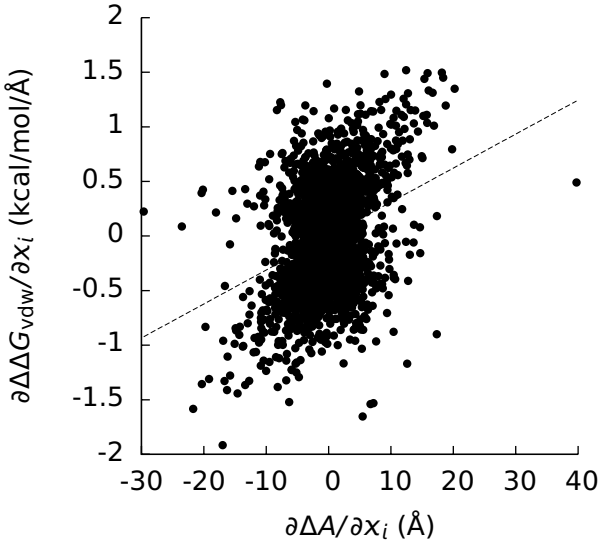
2
1.5
1
0.5
0
-0.5
-1
-1.5
-2
-30 -20 -10 0 10 20 30 40
$\partial\Delta\Delta G_{vdw}/\partial x_i$ (kcal/mol/Å)
$\partial\Delta A/\partial x_i$ (Å)

(d)

Figure 5: a) The derivative ($\partial \Delta G_{\mathrm{rep}} / \partial x_i$) of the repulsive component (ΔG_{rep}) of the Lennard-Jones cavity insertion free energy (ΔG_{vdw}) with respect to the coordinates (x_i) of the atomic centers versus the derivative ($\partial A / \partial x_i$) of the solvent-accessible area (A) with respect to x_i for the 1AVX complex. b) $\partial \Delta G_{\mathrm{vdw}} / \partial x_i$ versus $\partial A / \partial x_i$ for the 1AVX complex. c) The derivative ($\partial \Delta \Delta G_{\mathrm{rep}} / \partial x_i$) of the repulsive component ($\Delta \Delta G_{\mathrm{rep}}$) of the Lennard-Jones component ($\Delta \Delta G_{\mathrm{vdw}}$) of the binding free energy with respect to x_i versus the derivative ($\partial \Delta A / \partial x_i$) of the change ($\Delta A$) in A upon binding with respect to x_i for the 1AVX complex. d) $\partial \Delta \Delta G_{\mathrm{vdw}} / \partial x_i$ versus $\partial \Delta A / \partial x_i$ for the 1AVX complex. The dotted lines are least-squares lines drawn through the data. The slopes and squares of the Pearson correlation coefficients of these lines can be found in Table 1 of the main text.

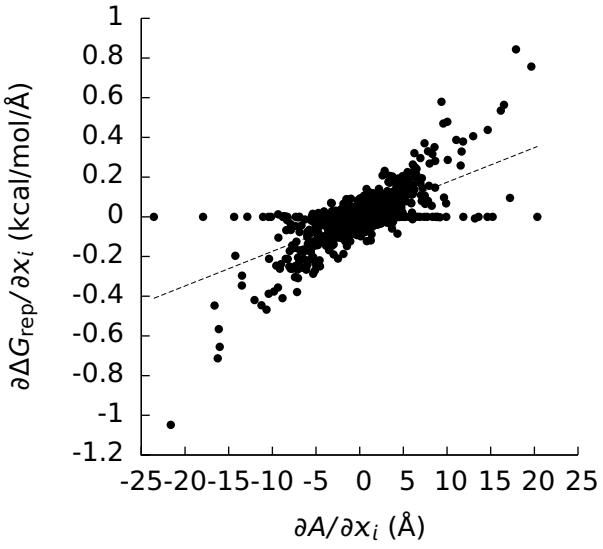
$\partial\Delta G_{rep}/\partial x_i$ (kcal/mol/Å)
$\partial A/\partial x_i$ (Å)

(a)

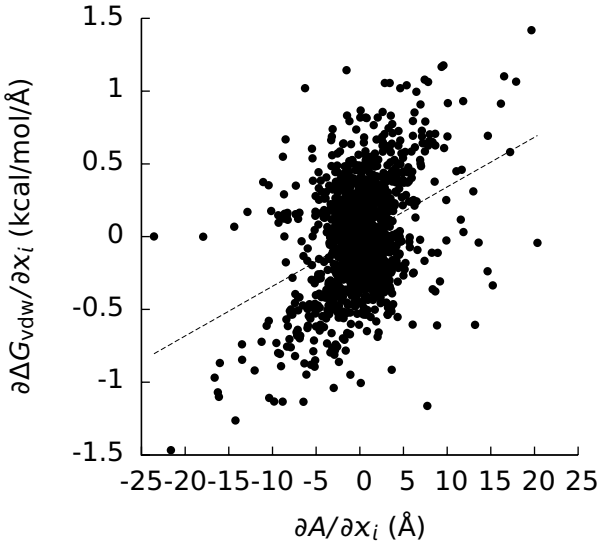
$\partial\Delta G_{vdw}/\partial x_i$ (kcal/mol/Å)
$\partial A/\partial x_i$ (Å)

(b)

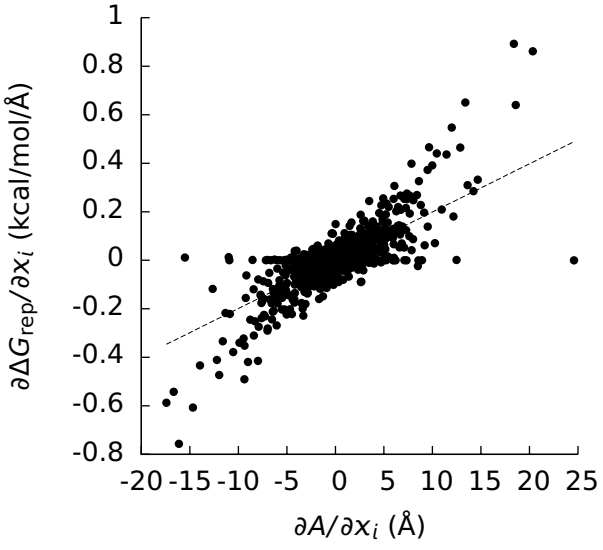
$\partial\Delta G_{rep}/\partial x_i$ (kcal/mol/Å)
$\partial A/\partial x_i$ (Å)

(c)

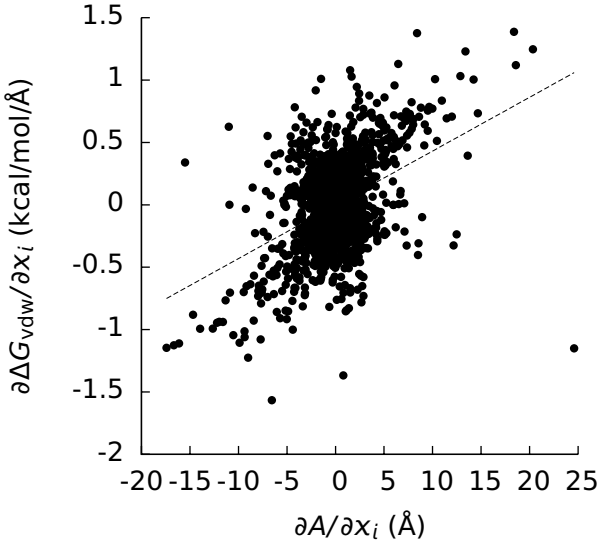
$\partial\Delta G_{vdw}/\partial x_i$ (kcal/mol/Å)
$\partial A/\partial x_i$ (Å)

(d)

Figure 6: a) The derivative ($\partial \Delta G_{\mathrm{rep}} / \partial x_i$) of the repulsive component (ΔG_{rep}) of the Lennard-Jones cavity insertion free energy (ΔG_{vdw}) with respect to the coordinates (x_i) of the atomic centers versus the derivative ($\partial A / \partial x_i$) of the solvent-accessible area (A) with respect to x_i for the first component of the 1BEB complex. b) $\partial \Delta G_{\mathrm{vdw}} / \partial x_i$ versus $\partial A / \partial x_i$ for the first component of the 1BEB complex. c) $\partial \Delta G_{\mathrm{rep}} / \partial x_i$ versus $\partial A / \partial x_i$ for the second component of the 1BEB complex. d) $\partial \Delta G_{\mathrm{vdw}} / \partial x_i$ versus $\partial A / \partial x_i$ for the second component of the 1BEB complex. The dotted lines are least-squares lines drawn through the data. The slopes and squares of the Pearson correlation coefficients of these lines can be found in Table 1 of the main text.

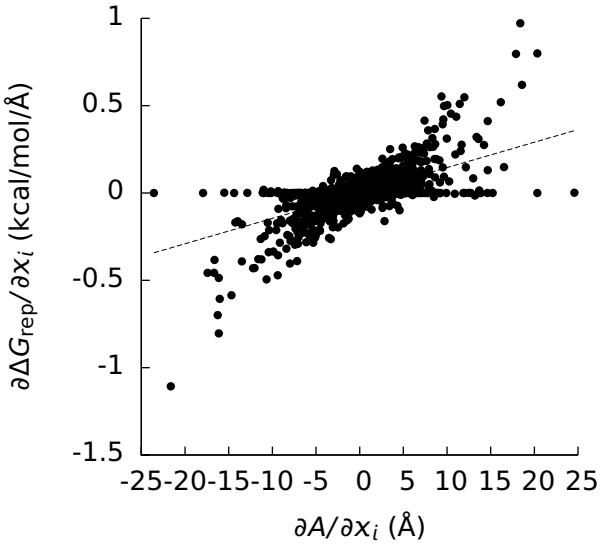
1
0.5
0
-0.5
-1
-1.5
-25-20-15-10 -5 0 5 10 15 20 25
$\partial\Delta G_{rep}/\partial x_i$ (kcal/mol/Å)
$\partial A/\partial x_i$ (Å)

(a)

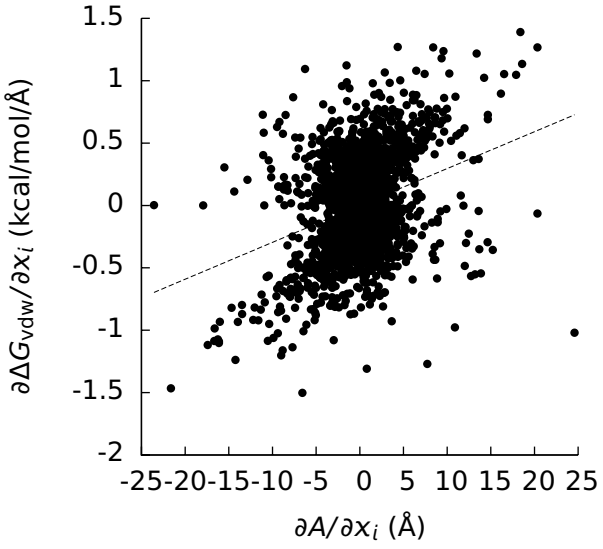
1.5
1
0.5
0
-0.5
-1
-1.5
-2
-25-20-15-10 -5 0 5 10 15 20 25
$\partial\Delta G_{vdw}/\partial x_i$ (kcal/mol/Å)
$\partial A/\partial x_i$ (Å)

(b)

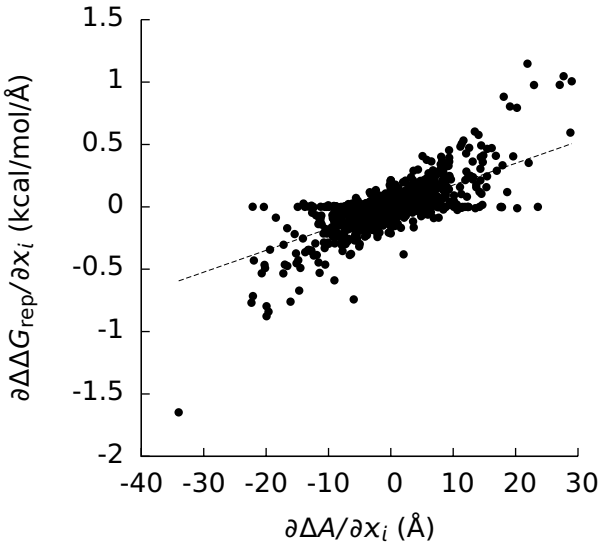
1.5
1
0.5
0
-0.5
-1
-1.5
-2
-40 -30 -20 -10 0 10 20 30
$\partial\Delta\Delta G_{rep}/\partial x_i$ (kcal/mol/Å)
$\partial\Delta A/\partial x_i$ (Å)

(c)

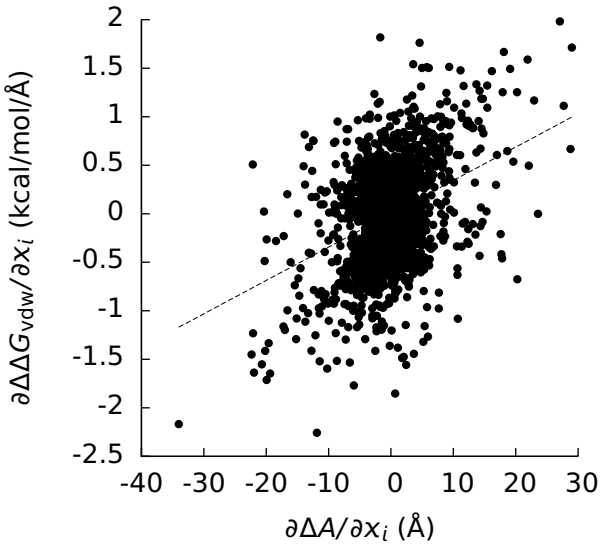
2
1.5
1
0.5
0
-0.5
-1
-1.5
-2
-2.5
-40 -30 -20 -10 0 10 20 30
$\partial\Delta\Delta G_{vdw}/\partial x_i$ (kcal/mol/Å)
$\partial\Delta A/\partial x_i$ (Å)

(d)

Figure 7: a) The derivative ($\partial \Delta G_{\mathrm{rep}} / \partial x_i$) of the repulsive component (ΔG_{rep}) of the Lennard-Jones cavity insertion free energy (ΔG_{vdw}) with respect to the coordinates (x_i) of the atomic centers versus the derivative ($\partial A / \partial x_i$) of the solvent-accessible area (A) with respect to x_i for the 1BEB complex. b) $\partial \Delta G_{\mathrm{vdw}} / \partial x_i$ versus $\partial A / \partial x_i$ for the 1BEB complex. c) The derivative ($\partial \Delta \Delta G_{\mathrm{rep}} / \partial x_i$) of the repulsive component ($\Delta \Delta G_{\mathrm{rep}}$) of the Lennard-Jones component ($\Delta \Delta G_{\mathrm{vdw}}$) of the binding free energy with respect to x_i versus the derivative ($\partial \Delta A / \partial x_i$) of the change ($\Delta A$) in A upon binding with respect to x_i for the 1BEB complex. d) $\partial \Delta \Delta G_{\mathrm{vdw}} / \partial x_i$ versus $\partial \Delta A / \partial x_i$ for the 1BEB complex. The dotted lines are least-squares lines drawn through the data. The slopes and squares of the Pearson correlation coefficients of these lines can be found in Table 1 of the main text.

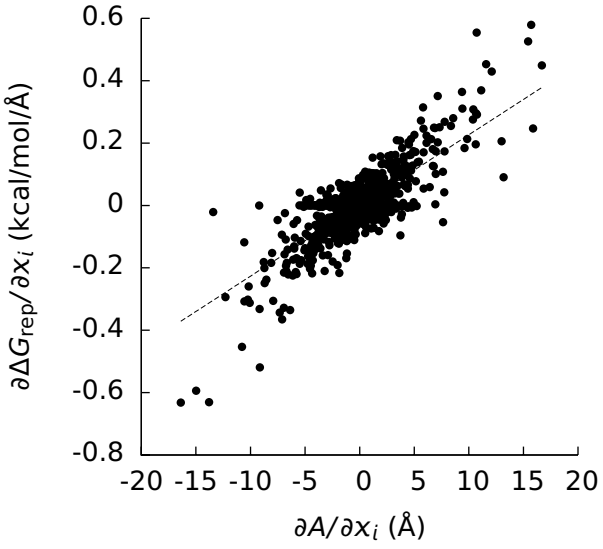
0.6
0.4
0.2
0
-0.2
-0.4
-0.6
-0.8
-20 -15 -10 -5 0 5 10 15 20
$\partial\Delta G_{rep}/\partial x_i$ (kcal/mol/Å)
$\partial A/\partial x_i$ (Å)

(a)

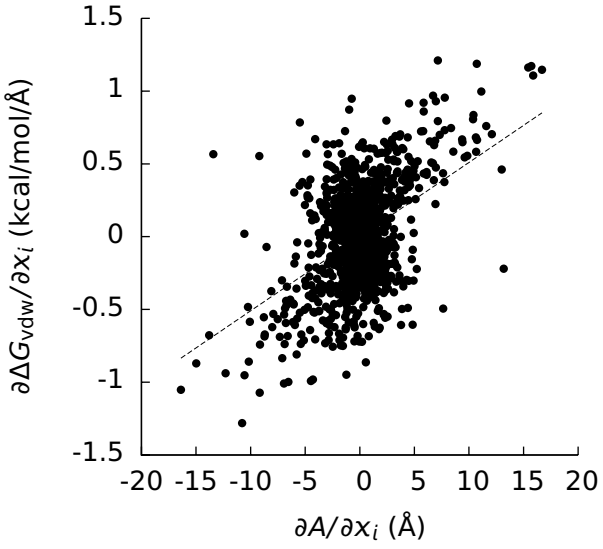
1.5
1
0.5
0
-0.5
-1
-1.5
-20 -15 -10 -5 0 5 10 15 20
$\partial\Delta G_{vdw}/\partial x_i$ (kcal/mol/Å)
$\partial A/\partial x_i$ (Å)

(b)

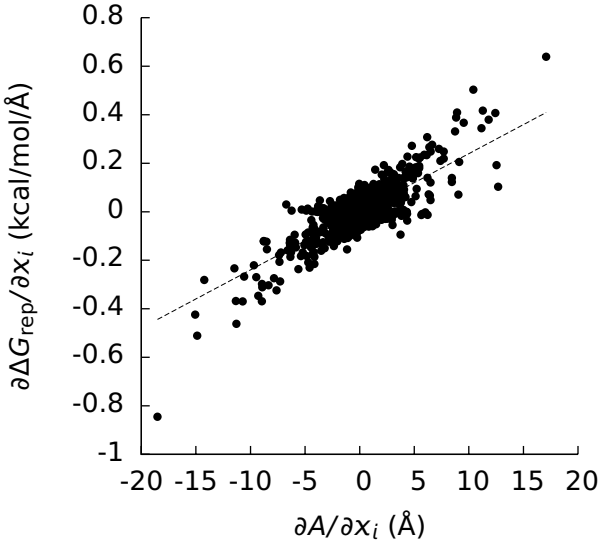
0.8
0.6
0.4
0.2
0
-0.2
-0.4
-0.6
-0.8
-1
-20 -15 -10 -5 0 5 10 15 20
$\partial\Delta G_{rep}/\partial x_i$ (kcal/mol/Å)
$\partial A/\partial x_i$ (Å)

(c)

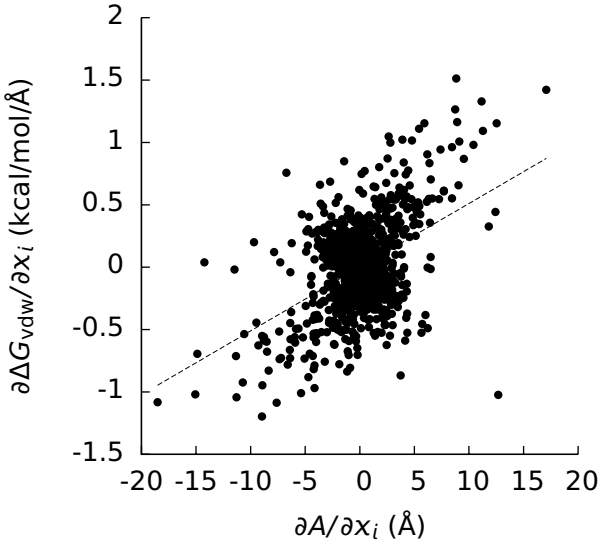
2
1.5
1
0.5
0
-0.5
-1
-1.5
-20 -15 -10 -5 0 5 10 15 20
$\partial\Delta G_{vdw}/\partial x_i$ (kcal/mol/Å)
$\partial A/\partial x_i$ (Å)

(d)

Figure 8: a) The derivative ($\partial \Delta G_{\mathrm{rep}} / \partial x_i$) of the repulsive component (ΔG_{rep}) of the Lennard-Jones cavity insertion free energy (ΔG_{vdw}) with respect to the coordinates (x_i) of the atomic centers versus the derivative ($\partial A / \partial x_i$) of the solvent-accessible area (A) with respect to x_i for the first component of the 1BRS complex. b) $\partial \Delta G_{\mathrm{vdw}} / \partial x_i$ versus $\partial A / \partial x_i$ for the first component of the 1BRS complex. c) $\partial \Delta G_{\mathrm{rep}} / \partial x_i$ versus $\partial A / \partial x_i$ for the second component of the 1BRS complex. d) $\partial \Delta G_{\mathrm{vdw}} / \partial x_i$ versus $\partial A / \partial x_i$ for the second component of the 1BRS complex. The dotted lines are least-squares lines drawn through the data. The slopes and squares of the Pearson correlation coefficients of these lines can be found in Table 1 of the main text.

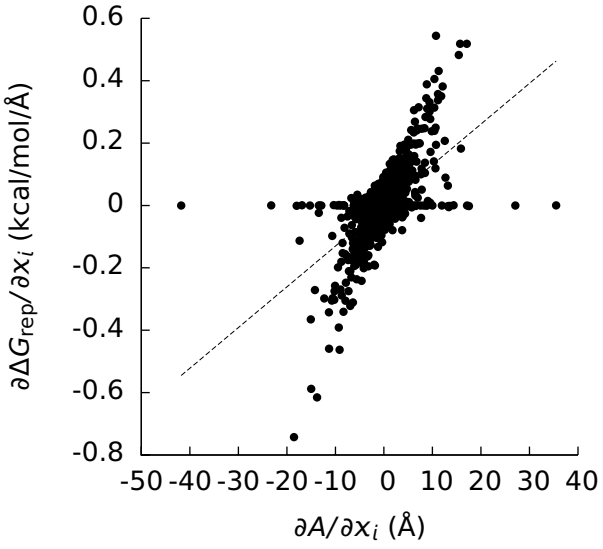
0.6
0.4
0.2
0
-0.2
-0.4
-0.6
-0.8
-50 -40 -30 -20 -10 0 10 20 30 40
$\partial\Delta G_{rep}/\partial x_i$ (kcal/mol/Å)
$\partial A/\partial x_i$ (Å)

(a)

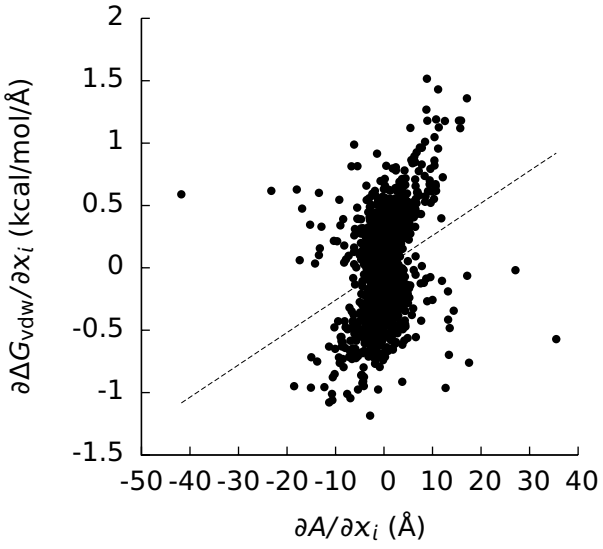
2
1.5
1
0.5
0
-0.5
-1
-1.5
-50 -40 -30 -20 -10 0 10 20 30 40
$\partial\Delta G_{vdw}/\partial x_i$ (kcal/mol/Å)
$\partial A/\partial x_i$ (Å)

(b)

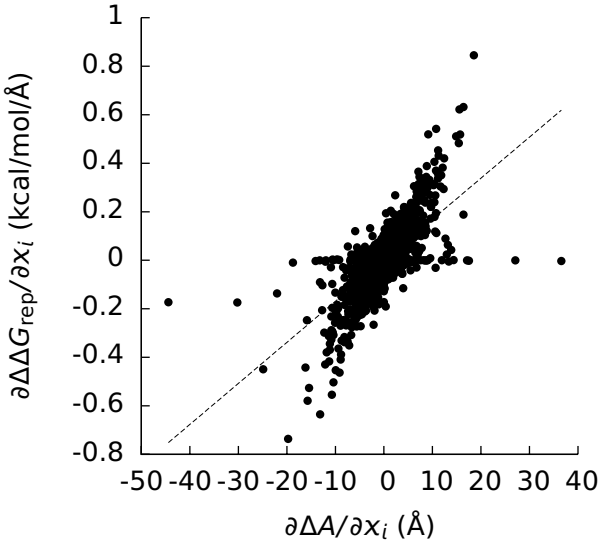
1
0.8
0.6
0.4
0.2
0
-0.2
-0.4
-0.6
-0.8
-50 -40 -30 -20 -10 0 10 20 30 40
$\partial\Delta\Delta G_{rep}/\partial x_i$ (kcal/mol/Å)
$\partial\Delta A/\partial x_i$ (Å)

(c)

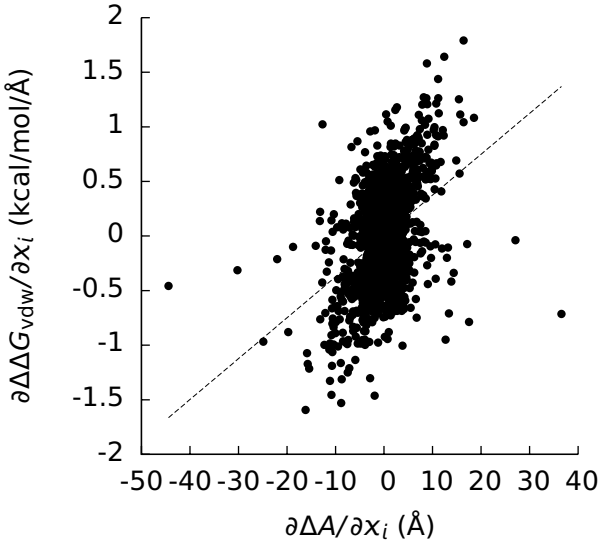
2
1.5
1
0.5
0
-0.5
-1
-1.5
-2
-50 -40 -30 -20 -10 0 10 20 30 40
$\partial\Delta\Delta G_{vdw}/\partial x_i$ (kcal/mol/Å)
$\partial\Delta A/\partial x_i$ (Å)

(d)

Figure 9: a) The derivative ($\partial \Delta G_{\mathrm{rep}} / \partial x_i$) of the repulsive component (ΔG_{rep}) of the Lennard-Jones cavity insertion free energy (ΔG_{vdw}) with respect to the coordinates (x_i) of the atomic centers versus the derivative ($\partial A / \partial x_i$) of the solvent-accessible area (A) with respect to x_i for the 1BRS complex. b) $\partial \Delta G_{\mathrm{vdw}} / \partial x_i$ versus $\partial A / \partial x_i$ for the 1BRS complex. c) The derivative ($\partial \Delta \Delta G_{\mathrm{rep}} / \partial x_i$) of the repulsive component ($\Delta \Delta G_{\mathrm{rep}}$) of the Lennard-Jones component ($\Delta \Delta G_{\mathrm{vdw}}$) of the binding free energy with respect to x_i versus the derivative ($\partial \Delta A / \partial x_i$) of the change ($\Delta A$) in A upon binding with respect to x_i for the 1BRS complex. d) $\partial \Delta \Delta G_{\mathrm{vdw}} / \partial x_i$ versus $\partial \Delta A / \partial x_i$ for the 1BRS complex. The dotted lines are least-squares lines drawn through the data. The slopes and squares of the Pearson correlation coefficients of these lines can be found in Table 1 of the main text.

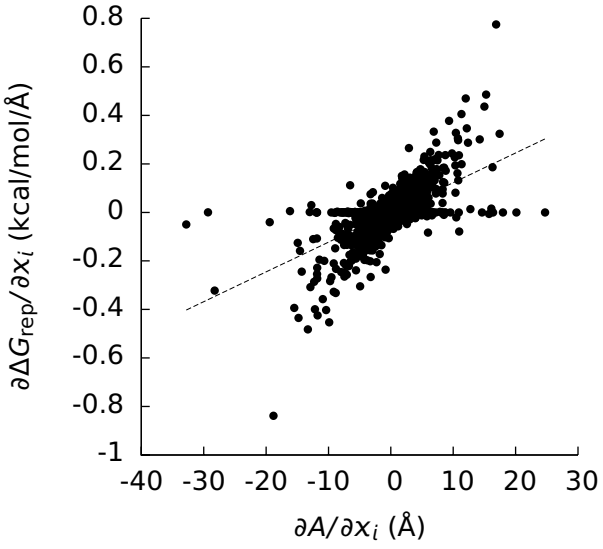
0.8
0.6
0.4
0.2
0
-0.2
-0.4
-0.6
-0.8
-1
-40 -30 -20 -10 0 10 20 30
$\partial\Delta G_{rep}/\partial x_i$ (kcal/mol/Å)
$\partial A/\partial x_i$ (Å)

(a)

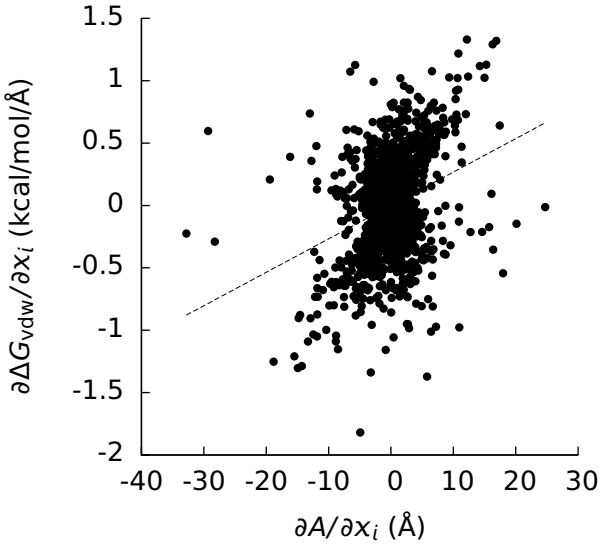
1.5
1
0.5
0
-0.5
-1
-1.5
-2
-40 -30 -20 -10 0 10 20 30
$\partial\Delta G_{vdw}/\partial x_i$ (kcal/mol/Å)
$\partial A/\partial x_i$ (Å)

(b)

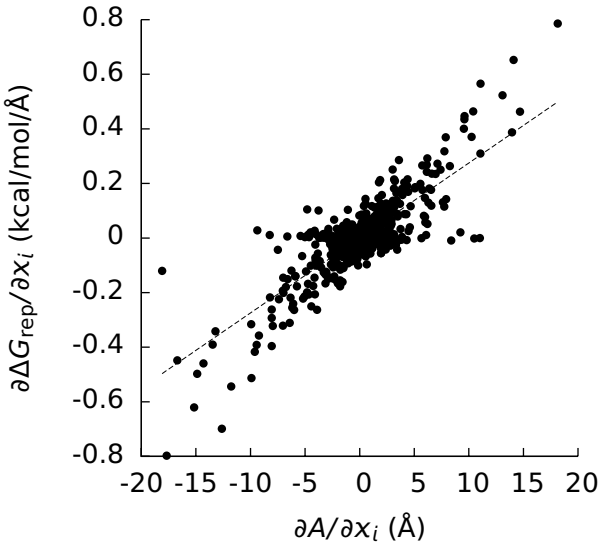
0.8
0.6
0.4
0.2
0
-0.2
-0.4
-0.6
-0.8
-20 -15 -10 -5 0 5 10 15 20
$\partial\Delta G_{rep}/\partial x_i$ (kcal/mol/Å)
$\partial A/\partial x_i$ (Å)

(c)

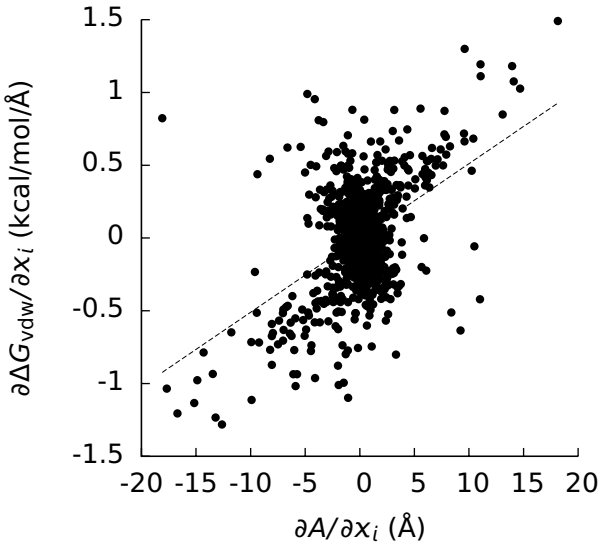
1.5
1
0.5
0
-0.5
-1
-1.5
-20 -15 -10 -5 0 5 10 15 20
$\partial\Delta G_{vdw}/\partial x_i$ (kcal/mol/Å)
$\partial A/\partial x_i$ (Å)

(d)

Figure 10: a) The derivative ($\partial \Delta G_{\mathrm{rep}} / \partial x_i$) of the repulsive component (ΔG_{rep}) of the Lennard-Jones cavity insertion free energy (ΔG_{vdw}) with respect to the coordinates (x_i) of the atomic centers versus the derivative ($\partial A / \partial x_i$) of the solvent-accessible area (A) with respect to x_i for the first component of the 1EAW complex. b) $\partial \Delta G_{\mathrm{vdw}} / \partial x_i$ versus $\partial A / \partial x_i$ for the first component of the 1EAW complex. c) $\partial \Delta G_{\mathrm{rep}} / \partial x_i$ versus $\partial A / \partial x_i$ for the second component of the 1EAW complex. d) $\partial \Delta G_{\mathrm{vdw}} / \partial x_i$ versus $\partial A / \partial x_i$ for the second component of the 1EAW complex. The dotted lines are least-squares lines drawn through the data. The slopes and squares of the Pearson correlation coefficients of these lines can be found in Table 1 of the main text.

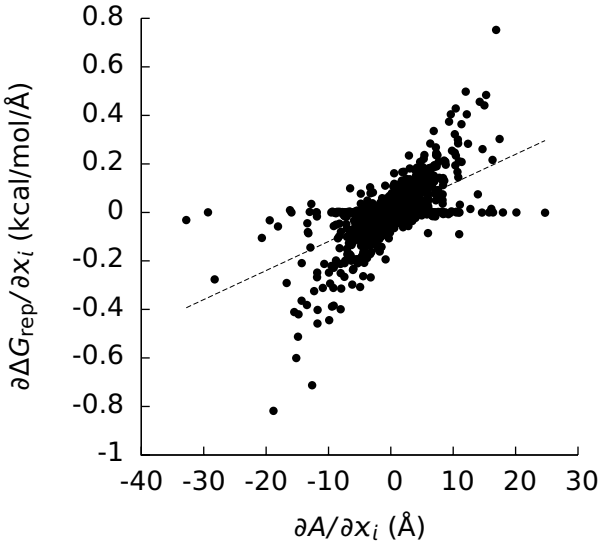
0.8
0.6
0.4
0.2
0
-0.2
-0.4
-0.6
-0.8
-1
-40 -30 -20 -10 0 10 20 30
$\partial\Delta G_{rep}/\partial x_i$ (kcal/mol/Å)
$\partial A/\partial x_i$ (Å)

(a)

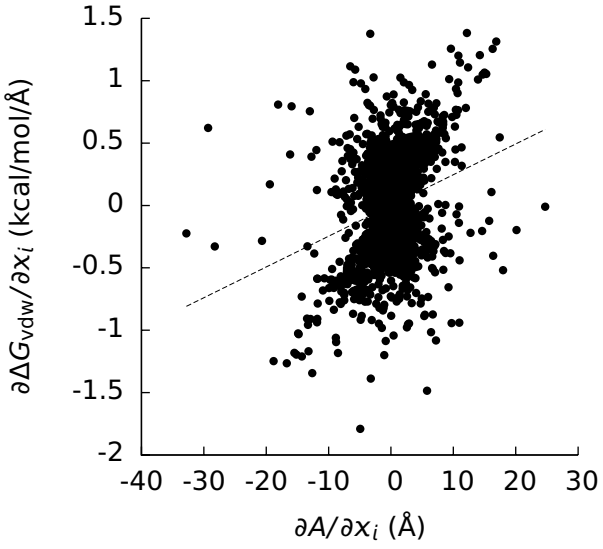
1.5
1
0.5
0
-0.5
-1
-1.5
-2
-40 -30 -20 -10 0 10 20 30
$\partial\Delta G_{vdw}/\partial x_i$ (kcal/mol/Å)
$\partial A/\partial x_i$ (Å)

(b)

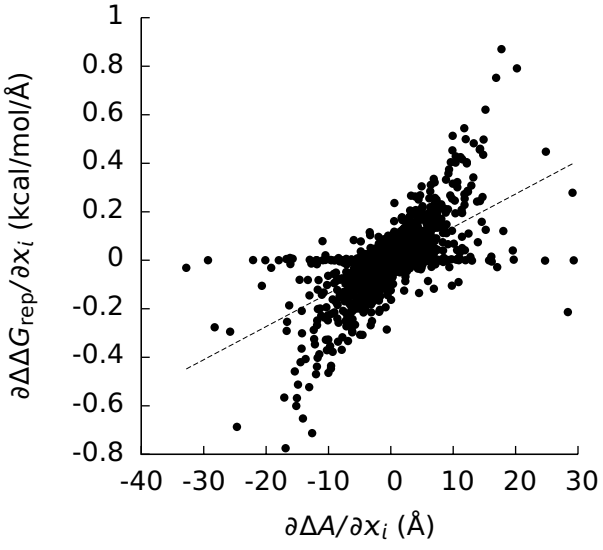
1
0.8
0.6
0.4
0.2
0
-0.2
-0.4
-0.6
-0.8
-40 -30 -20 -10 0 10 20 30
$\partial\Delta\Delta G_{rep}/\partial x_i$ (kcal/mol/Å)
$\partial\Delta A/\partial x_i$ (Å)

(c)

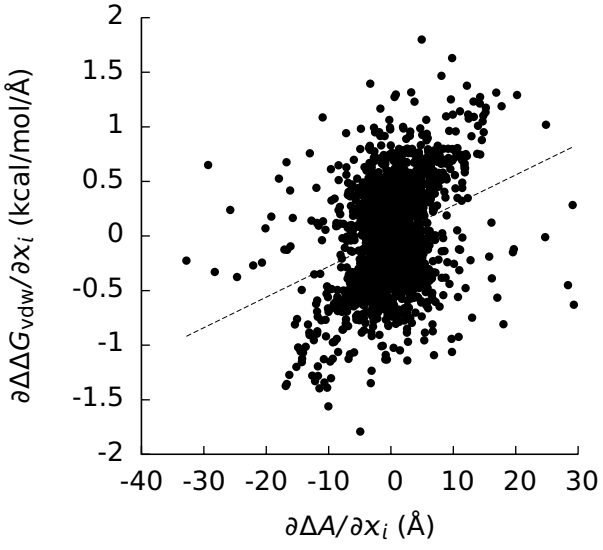
2
1.5
1
0.5
0
-0.5
-1
-1.5
-2
-40 -30 -20 -10 0 10 20 30
$\partial\Delta\Delta G_{vdw}/\partial x_i$ (kcal/mol/Å)
$\partial\Delta A/\partial x_i$ (Å)

(d)

Figure 11: a) The derivative ($\partial \Delta G_{\mathrm{rep}} / \partial x_i$) of the repulsive component (ΔG_{rep}) of the Lennard-Jones cavity insertion free energy (ΔG_{vdw}) with respect to the coordinates (x_i) of the atomic centers versus the derivative ($\partial A / \partial x_i$) of the solvent-accessible area (A) with respect to x_i for the 1EAW complex. b) $\partial \Delta G_{\mathrm{vdw}} / \partial x_i$ versus $\partial A / \partial x_i$ for the 1EAW complex. c) The derivative ($\partial \Delta \Delta G_{\mathrm{rep}} / \partial x_i$) of the repulsive component ($\Delta \Delta G_{\mathrm{rep}}$) of the Lennard-Jones component ($\Delta \Delta G_{\mathrm{vdw}}$) of the binding free energy with respect to x_i versus the derivative ($\partial \Delta A / \partial x_i$) of the change ($\Delta A$) in A upon binding with respect to x_i for the 1EAW complex. d) $\partial \Delta \Delta G_{\mathrm{vdw}} / \partial x_i$ versus $\partial \Delta A / \partial x_i$ for the 1EAW complex. The dotted lines are least-squares lines drawn through the data. The slopes and squares of the Pearson correlation coefficients of these lines can be found in Table 1 of the main text.

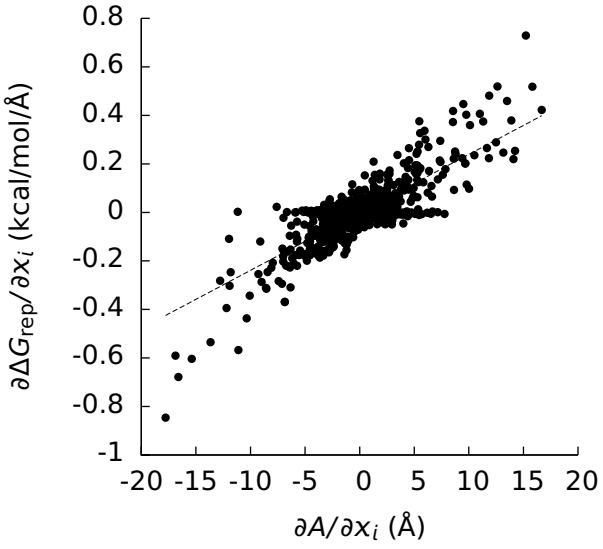
0.8
0.6
0.4
0.2
0
-0.2
-0.4
-0.6
-0.8
-1
-20 -15 -10 -5 0 5 10 15 20
$\partial\Delta G_{rep}/\partial x_i$ (kcal/mol/Å)
$\partial A/\partial x_i$ (Å)

(a)

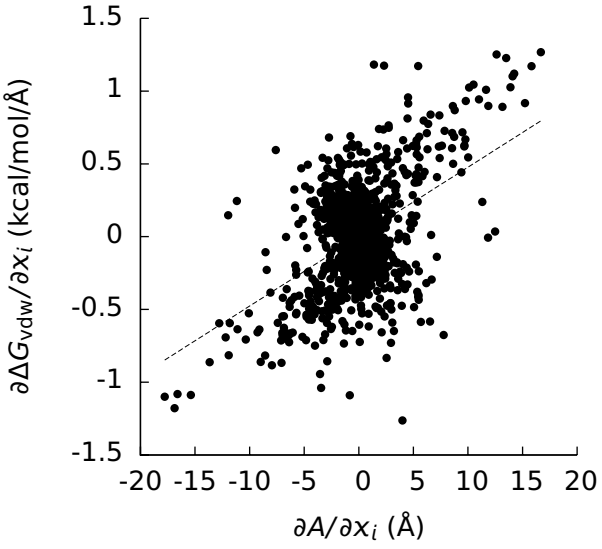
1.5
1
0.5
0
-0.5
-1
-1.5
-20 -15 -10 -5 0 5 10 15 20
$\partial\Delta G_{vdw}/\partial x_i$ (kcal/mol/Å)
$\partial A/\partial x_i$ (Å)

(b)

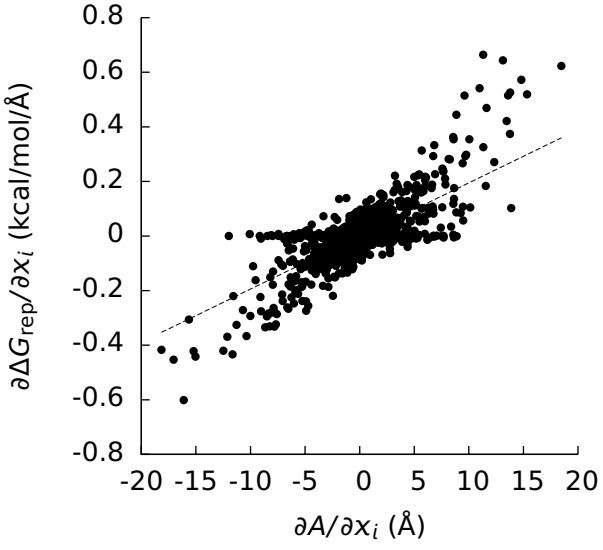
0.8
0.6
0.4
0.2
0
-0.2
-0.4
-0.6
-0.8
-20 -15 -10 -5 0 5 10 15 20
$\partial\Delta G_{rep}/\partial x_i$ (kcal/mol/Å)
$\partial A/\partial x_i$ (Å)

(c)

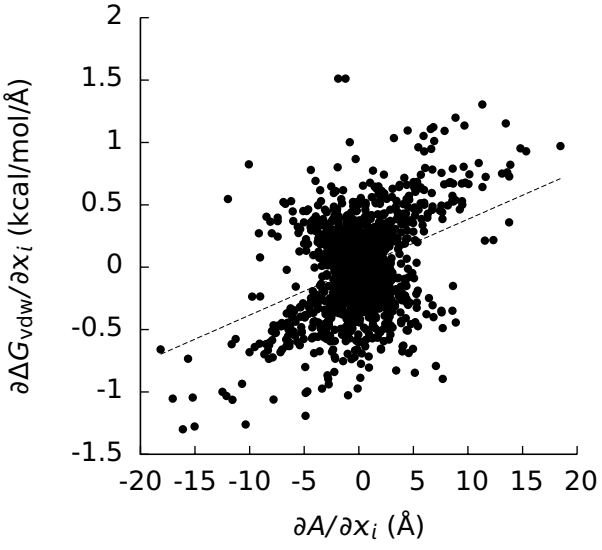
2
1.5
1
0.5
0
-0.5
-1
-1.5
-20 -15 -10 -5 0 5 10 15 20
$\partial\Delta G_{vdw}/\partial x_i$ (kcal/mol/Å)
$\partial A/\partial x_i$ (Å)

(d)

Figure 12: a) The derivative ($\partial \Delta G_{\mathrm{rep}} / \partial x_i$) of the repulsive component (ΔG_{rep}) of the Lennard-Jones cavity insertion free energy (ΔG_{vdw}) with respect to the coordinates (x_i) of the atomic centers versus the derivative ($\partial A / \partial x_i$) of the solvent-accessible area (A) with respect to x_i for the first component of the 1EMV complex. b) $\partial \Delta G_{\mathrm{vdw}} / \partial x_i$ versus $\partial A / \partial x_i$ for the first component of the 1EMV complex. c) $\partial \Delta G_{\mathrm{rep}} / \partial x_i$ versus $\partial A / \partial x_i$ for the second component of the 1EMV complex. d) $\partial \Delta G_{\mathrm{vdw}} / \partial x_i$ versus $\partial A / \partial x_i$ for the second component of the 1EMV complex. The dotted lines are least-squares lines drawn through the data. The slopes and squares of the Pearson correlation coefficients of these lines can be found in Table 1 of the main text.

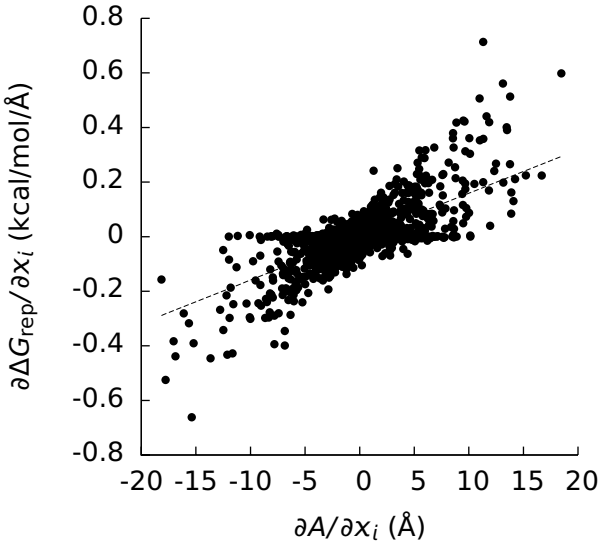
0.8
0.6
0.4
0.2
0
-0.2
-0.4
-0.6
-0.8
-20 -15 -10 -5 0 5 10 15 20
$\partial\Delta G_{rep}/\partial x_i$ (kcal/mol/Å)
$\partial A/\partial x_i$ (Å)

(a)

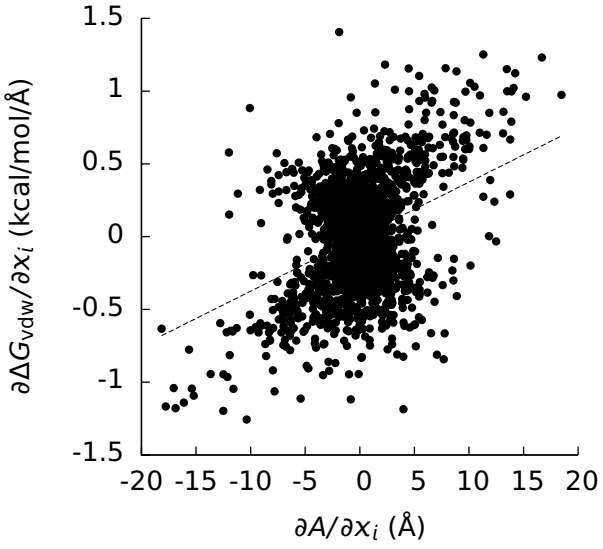
1.5
1
0.5
0
-0.5
-1
-1.5
-20 -15 -10 -5 0 5 10 15 20
$\partial\Delta G_{vdw}/\partial x_i$ (kcal/mol/Å)
$\partial A/\partial x_i$ (Å)

(b)

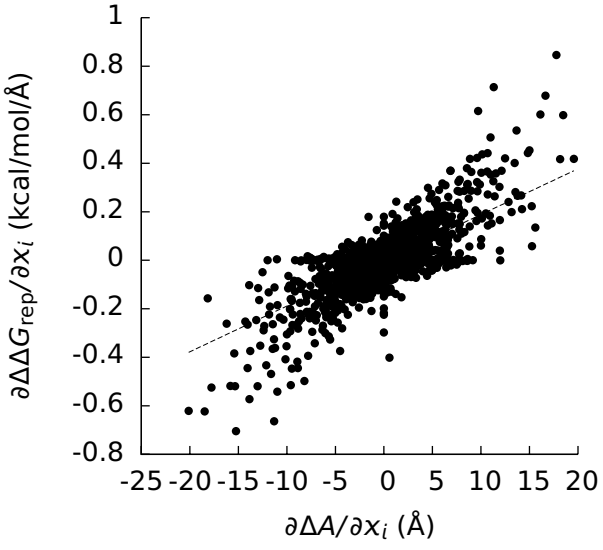
1
0.8
0.6
0.4
0.2
0
-0.2
-0.4
-0.6
-0.8
-25 -20 -15 -10 -5 0 5 10 15 20
$\partial\Delta\Delta G_{rep}/\partial x_i$ (kcal/mol/Å)
$\partial\Delta A/\partial x_i$ (Å)

(c)

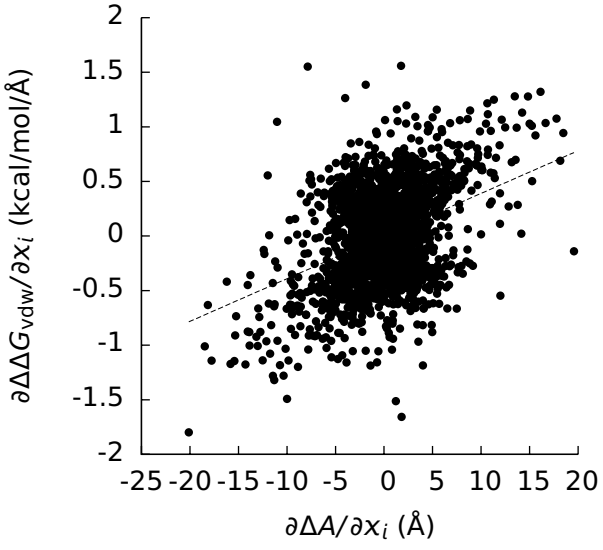
2
1.5
1
0.5
0
-0.5
-1
-1.5
-2
-25 -20 -15 -10 -5 0 5 10 15 20
$\partial\Delta\Delta G_{vdw}/\partial x_i$ (kcal/mol/Å)
$\partial\Delta A/\partial x_i$ (Å)

(d)

Figure 13: a) The derivative ($\partial \Delta G_{\mathrm{rep}} / \partial x_i$) of the repulsive component (ΔG_{rep}) of the Lennard-Jones cavity insertion free energy (ΔG_{vdw}) with respect to the coordinates (x_i) of the atomic centers versus the derivative ($\partial A / \partial x_i$) of the solvent-accessible area (A) with respect to x_i for the 1EMV complex. b) $\partial \Delta G_{\mathrm{vdw}} / \partial x_i$ versus $\partial A / \partial x_i$ for the 1EMV complex. c) The derivative ($\partial \Delta \Delta G_{\mathrm{rep}} / \partial x_i$) of the repulsive component ($\Delta \Delta G_{\mathrm{rep}}$) of the Lennard-Jones component ($\Delta \Delta G_{\mathrm{vdw}}$) of the binding free energy with respect to x_i versus the derivative ($\partial \Delta A / \partial x_i$) of the change ($\Delta A$) in A upon binding with respect to x_i for the 1EMV complex. d) $\partial \Delta \Delta G_{\mathrm{vdw}} / \partial x_i$ versus $\partial \Delta A / \partial x_i$ for the 1EMV complex. The dotted lines are least-squares lines drawn through the data. The slopes and squares of the Pearson correlation coefficients of these lines can be found in Table 1 of the main text.

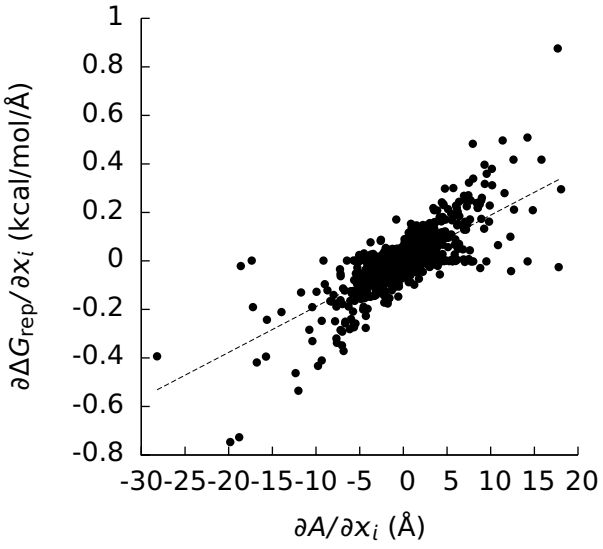
1
0.8
0.6
0.4
0.2
0
-0.2
-0.4
-0.6
-0.8
-30 -25 -20 -15 -10 -5 0 5 10 15 20
$\partial\Delta G_{rep}/\partial x_i$ (kcal/mol/Å)
$\partial A/\partial x_i$ (Å)

(a)

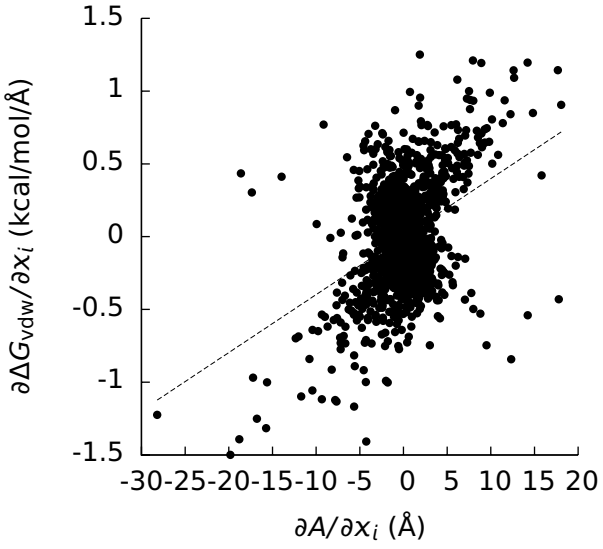
1.5
1
0.5
0
-0.5
-1
-1.5
-30 -25 -20 -15 -10 -5 0 5 10 15 20
$\partial\Delta G_{vdw}/\partial x_i$ (kcal/mol/Å)
$\partial A/\partial x_i$ (Å)

(b)

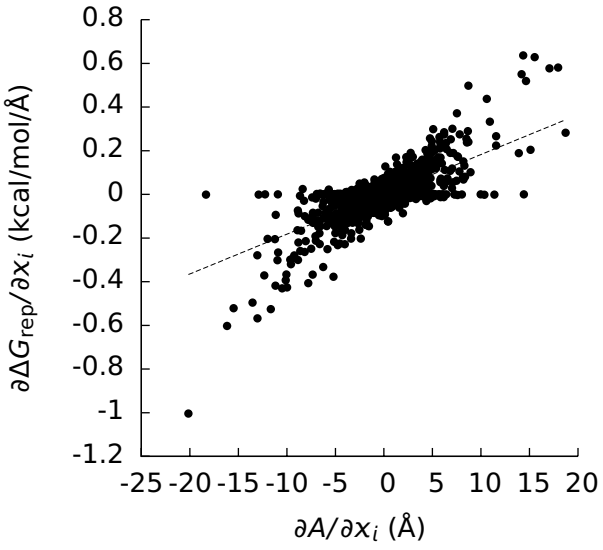
0.8
0.6
0.4
0.2
0
-0.2
-0.4
-0.6
-0.8
-1
-1.2
-25 -20 -15 -10 -5 0 5 10 15 20
$\partial\Delta G_{rep}/\partial x_i$ (kcal/mol/Å)
$\partial A/\partial x_i$ (Å)

(c)

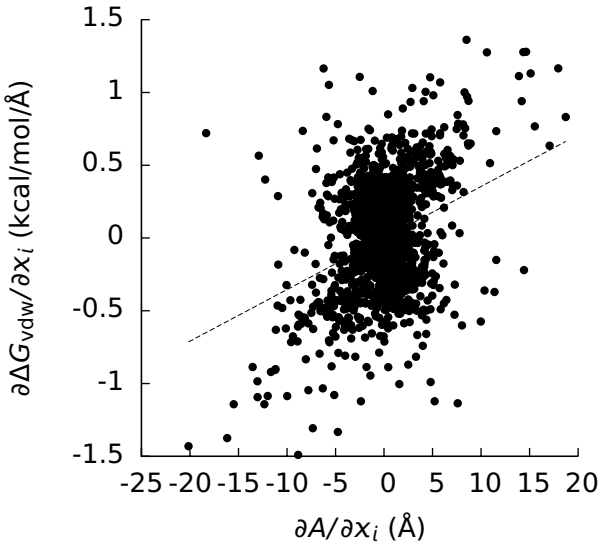
1.5
1
0.5
0
-0.5
-1
-1.5
-25 -20 -15 -10 -5 0 5 10 15 20
$\partial\Delta G_{vdw}/\partial x_i$ (kcal/mol/Å)
$\partial A/\partial x_i$ (Å)

(d)

Figure 14: a) The derivative ($\partial \Delta G_{\mathrm{rep}} / \partial x_i$) of the repulsive component (ΔG_{rep}) of the Lennard-Jones cavity insertion free energy (ΔG_{vdw}) with respect to the coordinates (x_i) of the atomic centers versus the derivative ($\partial A / \partial x_i$) of the solvent-accessible area (A) with respect to x_i for the first component of the 1HE1 complex. b) $\partial \Delta G_{\mathrm{vdw}} / \partial x_i$ versus $\partial A / \partial x_i$ for the first component of the 1HE1 complex. c) $\partial \Delta G_{\mathrm{rep}} / \partial x_i$ versus $\partial A / \partial x_i$ for the second component of the 1HE1 complex. d) $\partial \Delta G_{\mathrm{vdw}} / \partial x_i$ versus $\partial A / \partial x_i$ for the second component of the 1HE1 complex. The dotted lines are least-squares lines drawn through the data. The slopes and squares of the Pearson correlation coefficients of these lines can be found in Table 1 of the main text.

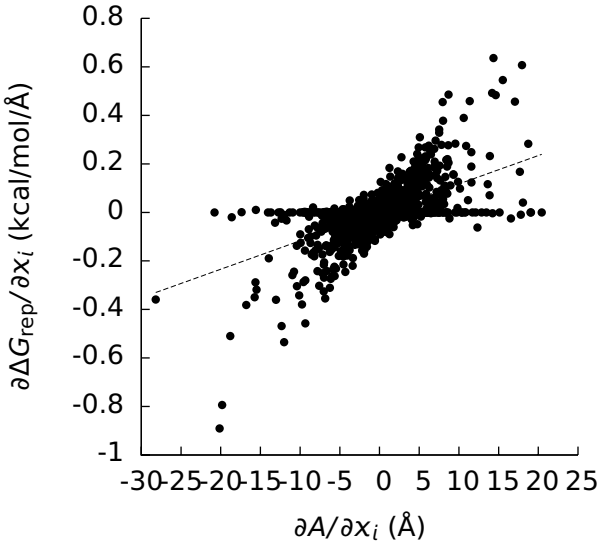
0.8
0.6
0.4
0.2
0
-0.2
-0.4
-0.6
-0.8
-1
-30 -25 -20 -15 -10 -5 0 5 10 15 20 25
$\partial\Delta G_{rep}/\partial x_i$ (kcal/mol/Å)
$\partial A/\partial x_i$ (Å)

(a)

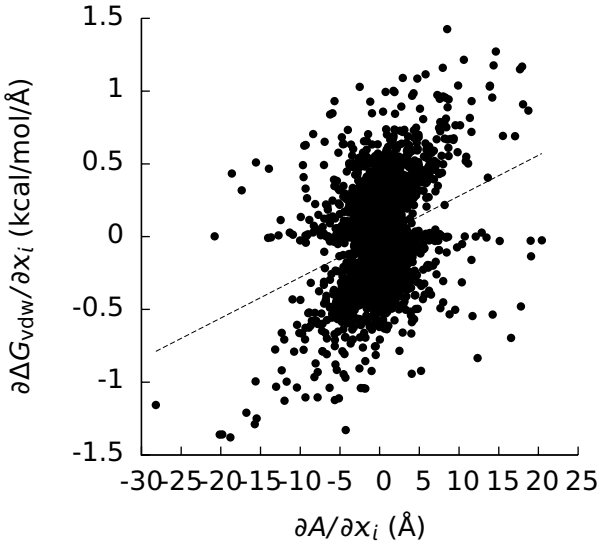
1.5
1
0.5
0
-0.5
-1
-1.5
-30 -25 -20 -15 -10 -5 0 5 10 15 20 25
$\partial\Delta G_{vdw}/\partial x_i$ (kcal/mol/Å)
$\partial A/\partial x_i$ (Å)

(b)

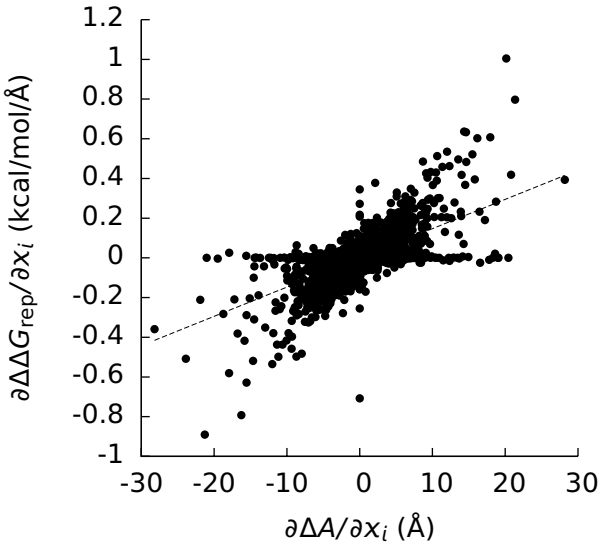
1.2
1
0.8
0.6
0.4
0.2
0
-0.2
-0.4
-0.6
-0.8
-1
-30 -20 -10 0 10 20 30
$\partial\Delta\Delta G_{rep}/\partial x_i$ (kcal/mol/Å)
$\partial\Delta A/\partial x_i$ (Å)

(c)

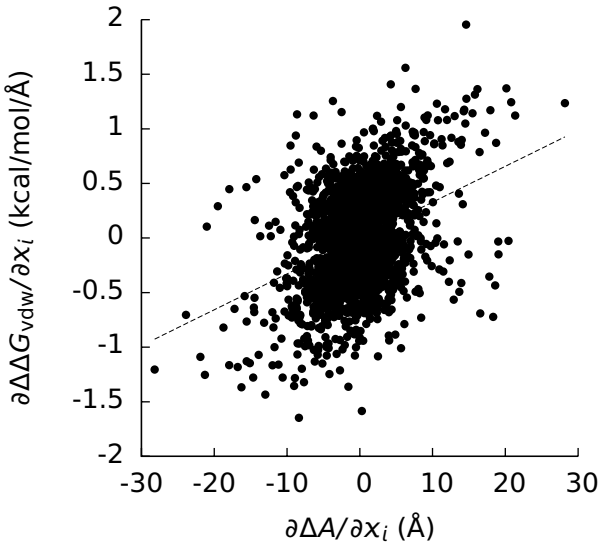
2
1.5
1
0.5
0
-0.5
-1
-1.5
-2
-30 -20 -10 0 10 20 30
$\partial\Delta\Delta G_{vdw}/\partial x_i$ (kcal/mol/Å)
$\partial\Delta A/\partial x_i$ (Å)

(d)

Figure 15: a) The derivative ($\partial \Delta G_{\mathrm{rep}} / \partial x_i$) of the repulsive component (ΔG_{rep}) of the Lennard-Jones cavity insertion free energy (ΔG_{vdw}) with respect to the coordinates (x_i) of the atomic centers versus the derivative ($\partial A / \partial x_i$) of the solvent-accessible area (A) with respect to x_i for the 1HE1 complex. b) $\partial \Delta G_{\mathrm{vdw}} / \partial x_i$ versus $\partial A / \partial x_i$ for the 1HE1 complex. c) The derivative ($\partial \Delta \Delta G_{\mathrm{rep}} / \partial x_i$) of the repulsive component ($\Delta \Delta G_{\mathrm{rep}}$) of the Lennard-Jones component ($\Delta \Delta G_{\mathrm{vdw}}$) of the binding free energy with respect to x_i versus the derivative ($\partial \Delta A / \partial x_i$) of the change ($\Delta A$) in A upon binding with respect to x_i for the 1HE1 complex. d) $\partial \Delta \Delta G_{\mathrm{vdw}} / \partial x_i$ versus $\partial \Delta A / \partial x_i$ for the 1HE1 complex. The dotted lines are least-squares lines drawn through the data. The slopes and squares of the Pearson correlation coefficients of these lines can be found in Table 1 of the main text.

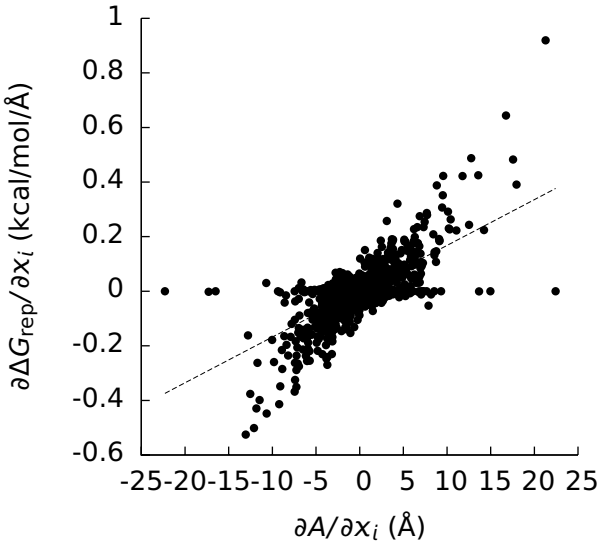
1
0.8
0.6
0.4
0.2
0
-0.2
-0.4
-0.6
-25 -20 -15 -10 -5 0 5 10 15 20 25
$\partial\Delta G_{rep}/\partial x_i$ (kcal/mol/Å)
$\partial A/\partial x_i$ (Å)

(a)

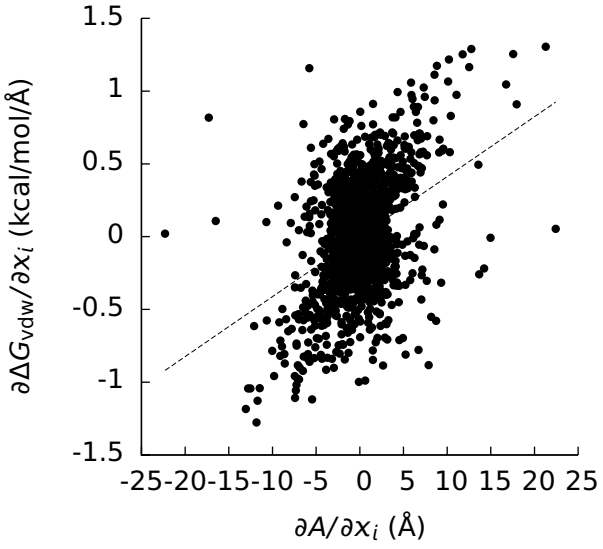
1.5
1
0.5
0
-0.5
-1
-1.5
-25 -20 -15 -10 -5 0 5 10 15 20 25
$\partial\Delta G_{vdw}/\partial x_i$ (kcal/mol/Å)
$\partial A/\partial x_i$ (Å)

(b)

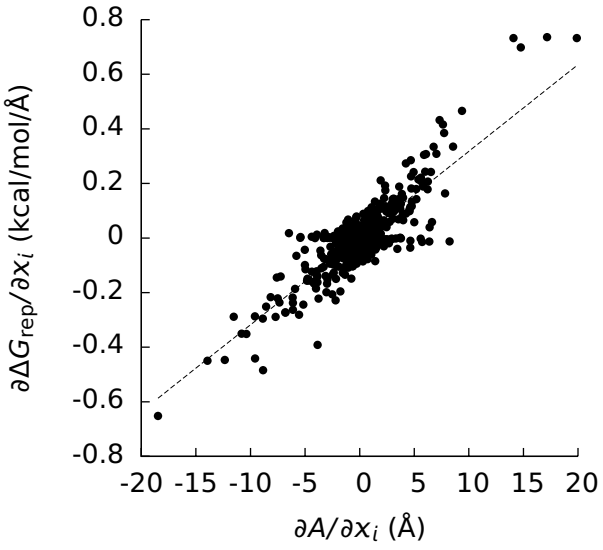
0.8
0.6
0.4
0.2
0
-0.2
-0.4
-0.6
-0.8
-20 -15 -10 -5 0 5 10 15 20
$\partial\Delta G_{rep}/\partial x_i$ (kcal/mol/Å)
$\partial A/\partial x_i$ (Å)

(c)

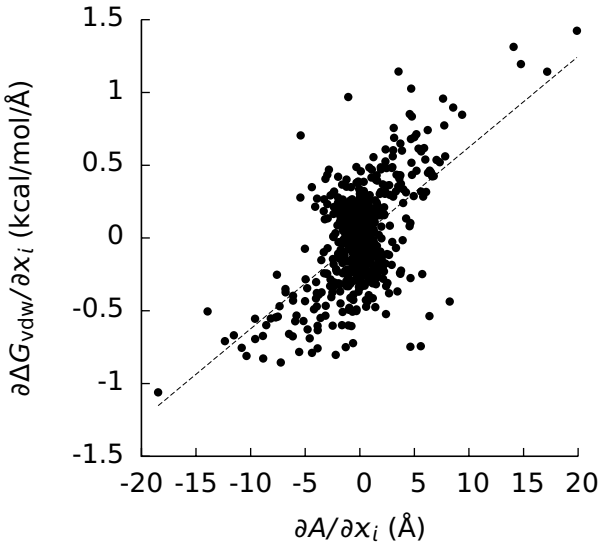
1.5
1
0.5
0
-0.5
-1
-1.5
-20 -15 -10 -5 0 5 10 15 20
$\partial\Delta G_{vdw}/\partial x_i$ (kcal/mol/Å)
$\partial A/\partial x_i$ (Å)

(d)

Figure 16: a) The derivative ($\partial \Delta G_{\mathrm{rep}} / \partial x_i$) of the repulsive component (ΔG_{rep}) of the Lennard-Jones cavity insertion free energy (ΔG_{vdw}) with respect to the coordinates (x_i) of the atomic centers versus the derivative ($\partial A / \partial x_i$) of the solvent-accessible area (A) with respect to x_i for the first component of the 1PPE complex. b) $\partial \Delta G_{\mathrm{vdw}} / \partial x_i$ versus $\partial A / \partial x_i$ for the first component of the 1PPE complex. c) $\partial \Delta G_{\mathrm{rep}} / \partial x_i$ versus $\partial A / \partial x_i$ for the second component of the 1PPE complex. d) $\partial \Delta G_{\mathrm{vdw}} / \partial x_i$ versus $\partial A / \partial x_i$ for the second component of the 1PPE complex. The dotted lines are least-squares lines drawn through the data. The slopes and squares of the Pearson correlation coefficients of these lines can be found in Table 1 of the main text.

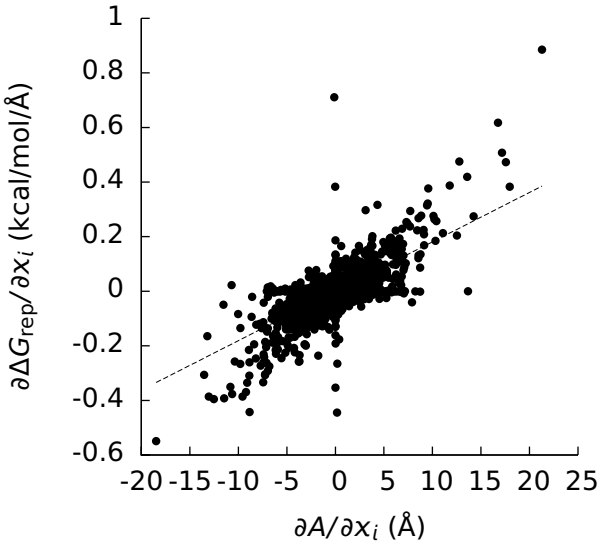
$\partial\Delta G_{rep}/\partial x_i$ (kcal/mol/Å)
$\partial A/\partial x_i$ (Å)

(a)

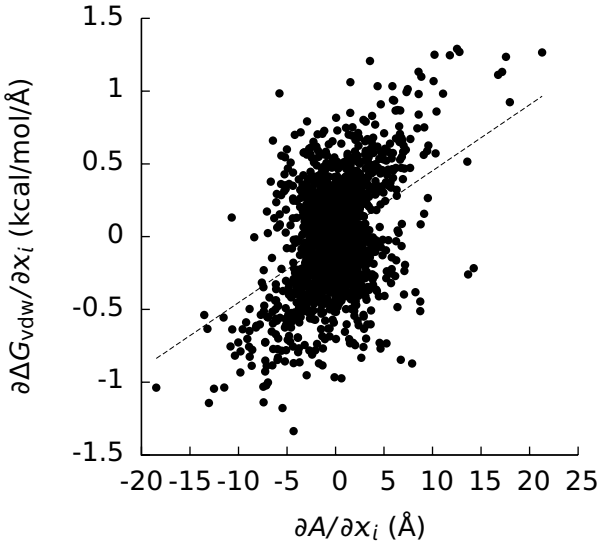
$\partial\Delta G_{vdw}/\partial x_i$ (kcal/mol/Å)
$\partial A/\partial x_i$ (Å)

(b)

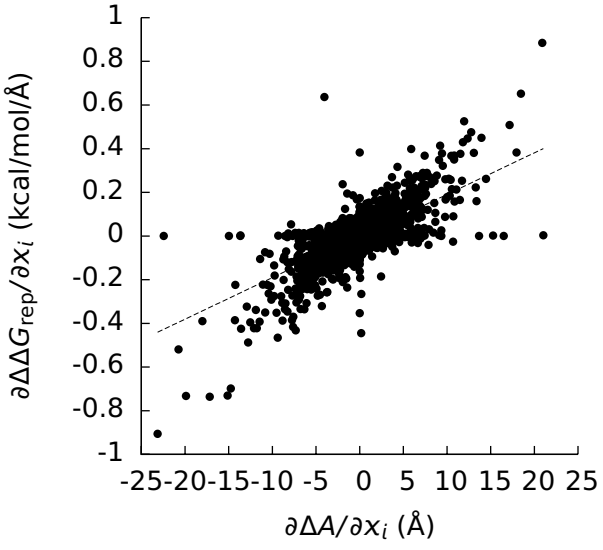
$\partial\Delta\Delta G_{rep}/\partial x_i$ (kcal/mol/Å)
$\partial\Delta A/\partial x_i$ (Å)

(c)

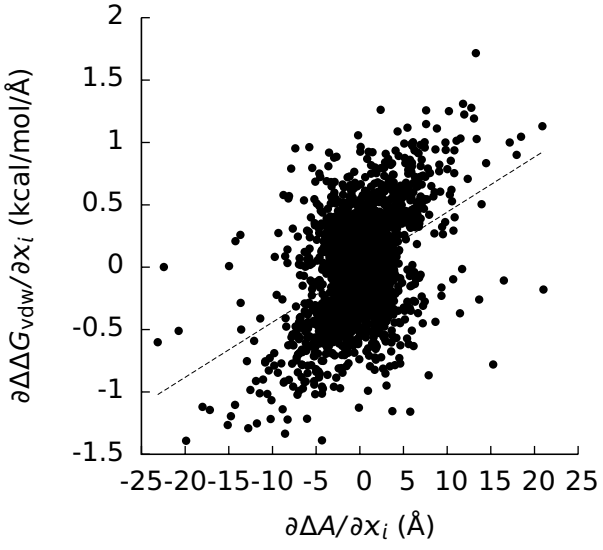
$\partial\Delta\Delta G_{vdw}/\partial x_i$ (kcal/mol/Å)
$\partial\Delta A/\partial x_i$ (Å)

(d)

Figure 17: a) The derivative ($\partial \Delta G_{\mathrm{rep}} / \partial x_i$) of the repulsive component (ΔG_{rep}) of the Lennard-Jones cavity insertion free energy (ΔG_{vdw}) with respect to the coordinates (x_i) of the atomic centers versus the derivative ($\partial A / \partial x_i$) of the solvent-accessible area (A) with respect to x_i for the 1PPE complex. b) $\partial \Delta G_{\mathrm{vdw}} / \partial x_i$ versus $\partial A / \partial x_i$ for the 1PPE complex. c) The derivative ($\partial \Delta \Delta G_{\mathrm{rep}} / \partial x_i$) of the repulsive component ($\Delta \Delta G_{\mathrm{rep}}$) of the Lennard-Jones component ($\Delta \Delta G_{\mathrm{vdw}}$) of the binding free energy with respect to x_i versus the derivative ($\partial \Delta A / \partial x_i$) of the change ($\Delta A$) in A upon binding with respect to x_i for the 1PPE complex. d) $\partial \Delta \Delta G_{\mathrm{vdw}} / \partial x_i$ versus $\partial \Delta A / \partial x_i$ for the 1PPE complex. The dotted lines are least-squares lines drawn through the data. The slopes and squares of the Pearson correlation coefficients of these lines can be found in Table 1 of the main text.

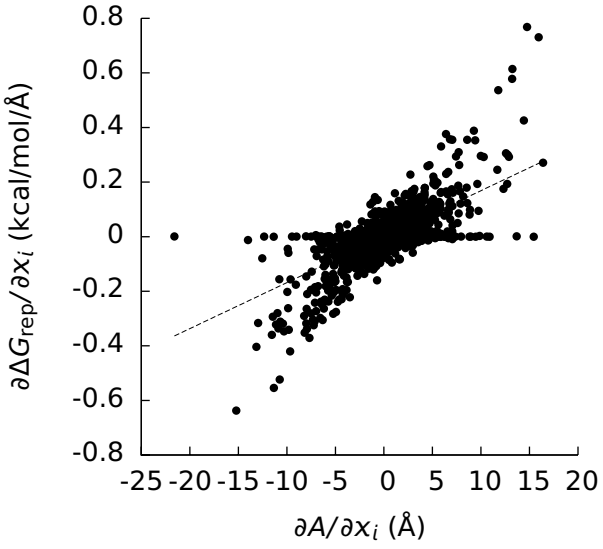
0.8
0.6
0.4
0.2
0
-0.2
-0.4
-0.6
-0.8
-25 -20 -15 -10 -5 0 5 10 15 20
$\partial\Delta G_{rep}/\partial x_i$ (kcal/mol/Å)
$\partial A/\partial x_i$ (Å)

(a)

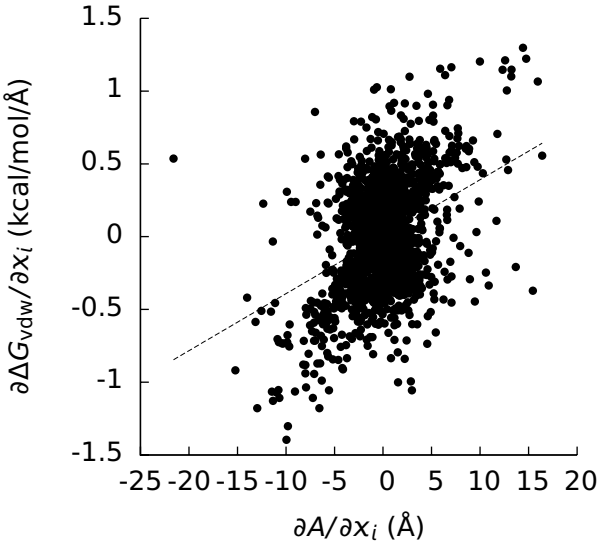
1.5
1
0.5
0
-0.5
-1
-1.5
-25 -20 -15 -10 -5 0 5 10 15 20
$\partial\Delta G_{vdw}/\partial x_i$ (kcal/mol/Å)
$\partial A/\partial x_i$ (Å)

(b)

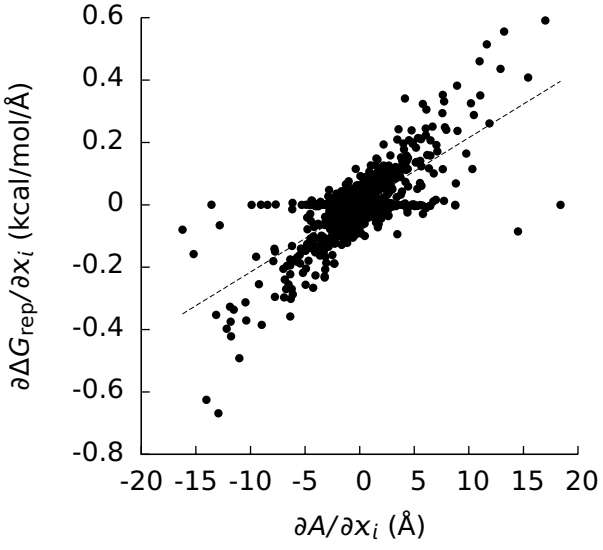
0.6
0.4
0.2
0
-0.2
-0.4
-0.6
-0.8
-20 -15 -10 -5 0 5 10 15 20
$\partial\Delta G_{rep}/\partial x_i$ (kcal/mol/Å)
$\partial A/\partial x_i$ (Å)

(c)

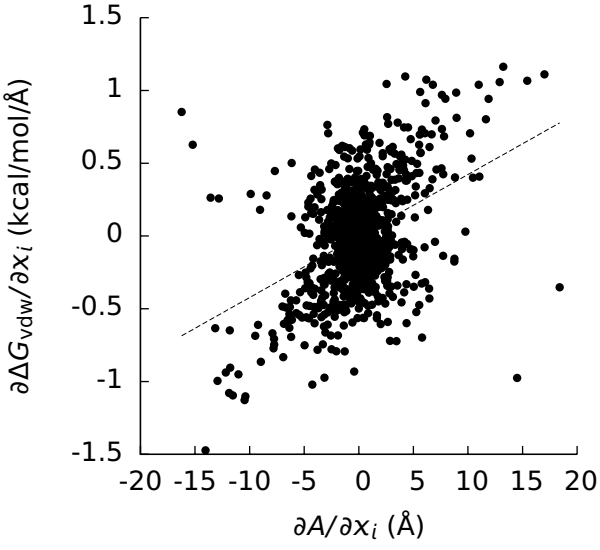
1.5
1
0.5
0
-0.5
-1
-1.5
-20 -15 -10 -5 0 5 10 15 20
$\partial\Delta G_{vdw}/\partial x_i$ (kcal/mol/Å)
$\partial A/\partial x_i$ (Å)

(d)

Figure 18: a) The derivative ($\partial \Delta G_{\mathrm{rep}} / \partial x_i$) of the repulsive component (ΔG_{rep}) of the Lennard-Jones cavity insertion free energy (ΔG_{vdw}) with respect to the coordinates (x_i) of the atomic centers versus the derivative ($\partial A / \partial x_i$) of the solvent-accessible area (A) with respect to x_i for the first component of the 1UDI complex. b) $\partial \Delta G_{\mathrm{vdw}} / \partial x_i$ versus $\partial A / \partial x_i$ for the first component of the 1UDI complex. c) $\partial \Delta G_{\mathrm{rep}} / \partial x_i$ versus $\partial A / \partial x_i$ for the second component of the 1UDI complex. d) $\partial \Delta G_{\mathrm{vdw}} / \partial x_i$ versus $\partial A / \partial x_i$ for the second component of the 1UDI complex. The dotted lines are least-squares lines drawn through the data. The slopes and squares of the Pearson correlation coefficients of these lines can be found in Table 1 of the main text.

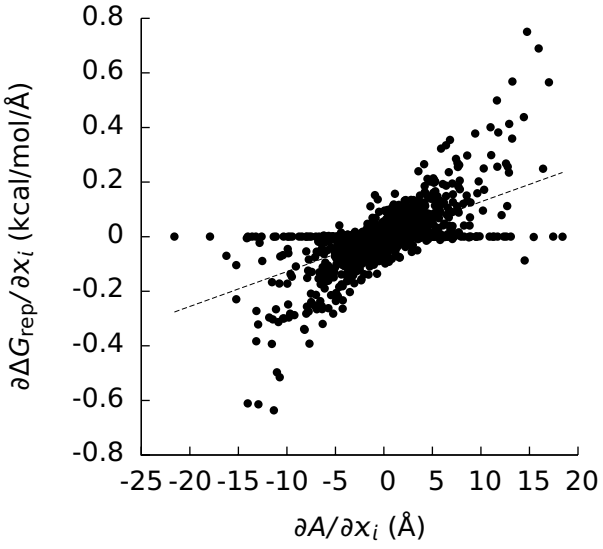
0.8
0.6
0.4
0.2
0
-0.2
-0.4
-0.6
-0.8
-25 -20 -15 -10 -5 0 5 10 15 20
$\partial\Delta G_{rep}/\partial x_i$ (kcal/mol/Å)
$\partial A/\partial x_i$ (Å)

(a)

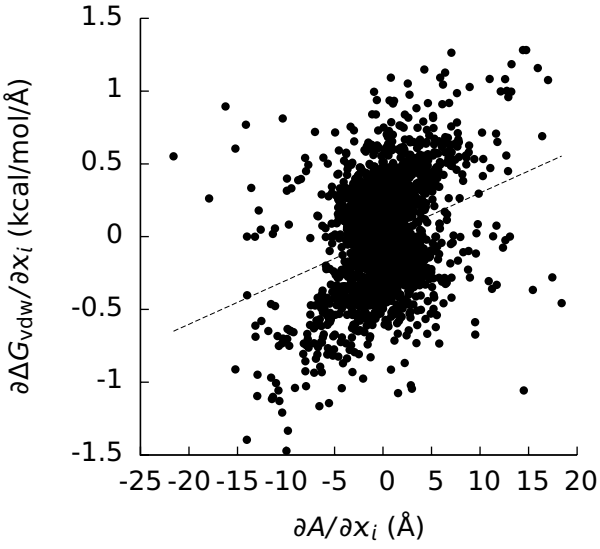
1.5
1
0.5
0
-0.5
-1
-1.5
-25 -20 -15 -10 -5 0 5 10 15 20
$\partial\Delta G_{vdw}/\partial x_i$ (kcal/mol/Å)
$\partial A/\partial x_i$ (Å)

(b)

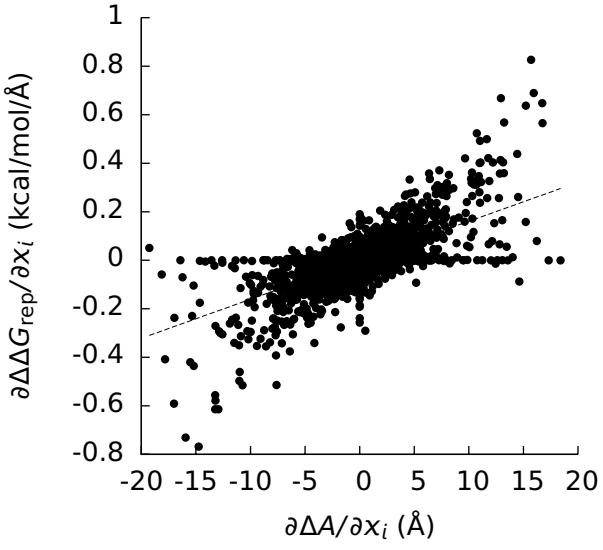
1
0.8
0.6
0.4
0.2
0
-0.2
-0.4
-0.6
-0.8
-20 -15 -10 -5 0 5 10 15 20
$\partial\Delta\Delta G_{rep}/\partial x_i$ (kcal/mol/Å)
$\partial\Delta A/\partial x_i$ (Å)

(c)

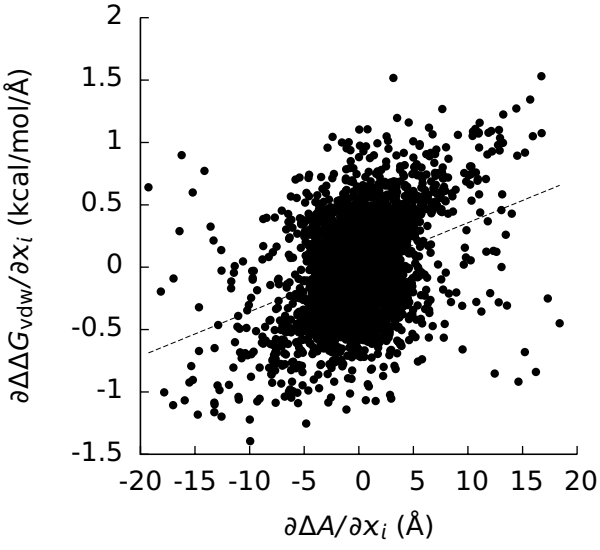
2
1.5
1
0.5
0
-0.5
-1
-1.5
-20 -15 -10 -5 0 5 10 15 20
$\partial\Delta\Delta G_{vdw}/\partial x_i$ (kcal/mol/Å)
$\partial\Delta A/\partial x_i$ (Å)

(d)

Figure 19: a) The derivative ($\partial \Delta G_{\mathrm{rep}} / \partial x_i$) of the repulsive component (ΔG_{rep}) of the Lennard-Jones cavity insertion free energy (ΔG_{vdw}) with respect to the coordinates (x_i) of the atomic centers versus the derivative ($\partial A / \partial x_i$) of the solvent-accessible area (A) with respect to x_i for the 1UDI complex. b) $\partial \Delta G_{\mathrm{vdw}} / \partial x_i$ versus $\partial A / \partial x_i$ for the 1UDI complex. c) The derivative ($\partial \Delta \Delta G_{\mathrm{rep}} / \partial x_i$) of the repulsive component ($\Delta \Delta G_{\mathrm{rep}}$) of the Lennard-Jones component ($\Delta \Delta G_{\mathrm{vdw}}$) of the binding free energy with respect to x_i versus the derivative ($\partial \Delta A / \partial x_i$) of the change ($\Delta A$) in A upon binding with respect to x_i for the 1UDI complex. d) $\partial \Delta \Delta G_{\mathrm{vdw}} / \partial x_i$ versus $\partial \Delta A / \partial x_i$ for the 1UDI complex. The dotted lines are least-squares lines drawn through the data. The slopes and squares of the Pearson correlation coefficients of these lines can be found in Table 1 of the main text.

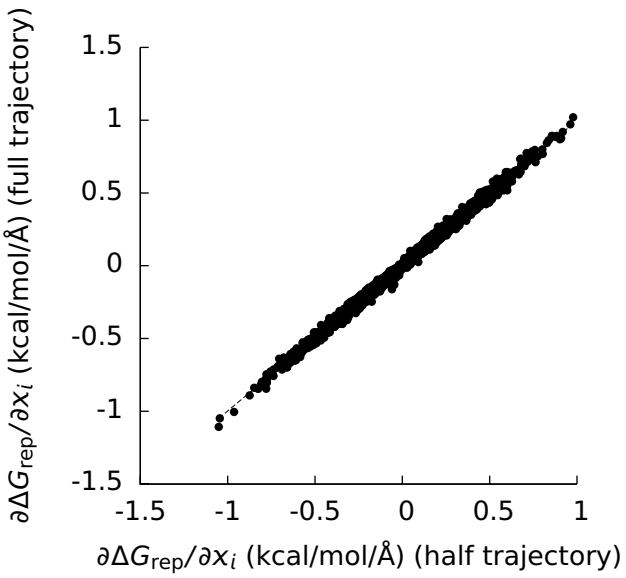
1.5
1
0.5
0
-0.5
-1
-1.5
-1.5 -1 -0.5 0 0.5 1
$\partial\Delta G_{\mathrm{rep}}/\partial x_i$ (kcal/mol/Å) (full trajectory)
$\partial\Delta G_{\mathrm{rep}}/\partial x_i$ (kcal/mol/Å) (half trajectory)

(a)

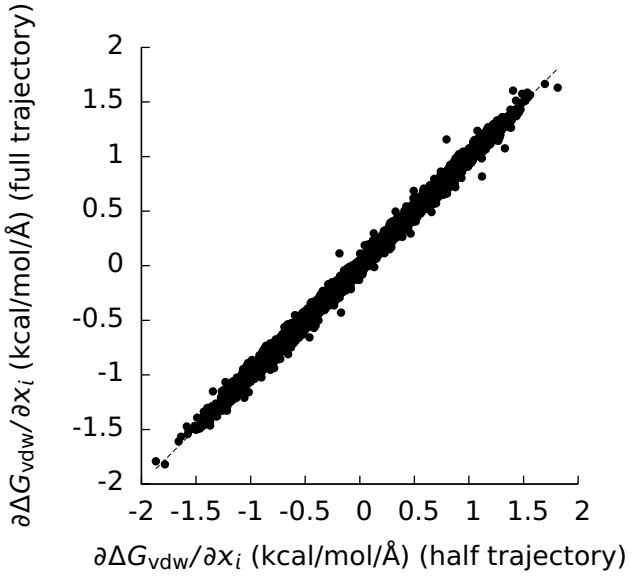
2
1.5
1
0.5
0
-0.5
-1
-1.5
-2
-2 -1.5 -1 -0.5 0 0.5 1 1.5 2
$\partial\Delta G_{\mathrm{vdw}}/\partial x_i$ (kcal/mol/Å) (full trajectory)
$\partial\Delta G_{\mathrm{vdw}}/\partial x_i$ (kcal/mol/Å) (half trajectory)

(b)

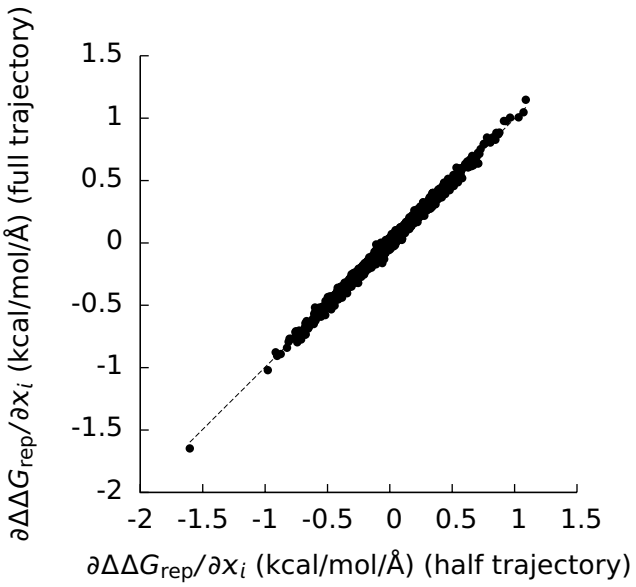
1.5
1
0.5
0
-0.5
-1
-1.5
-2
-2 -1.5 -1 -0.5 0 0.5 1 1.5
$\partial\Delta\Delta G_{\mathrm{rep}}/\partial x_i$ (kcal/mol/Å) (full trajectory)
$\partial\Delta\Delta G_{\mathrm{rep}}/\partial x_i$ (kcal/mol/Å) (half trajectory)

(c)

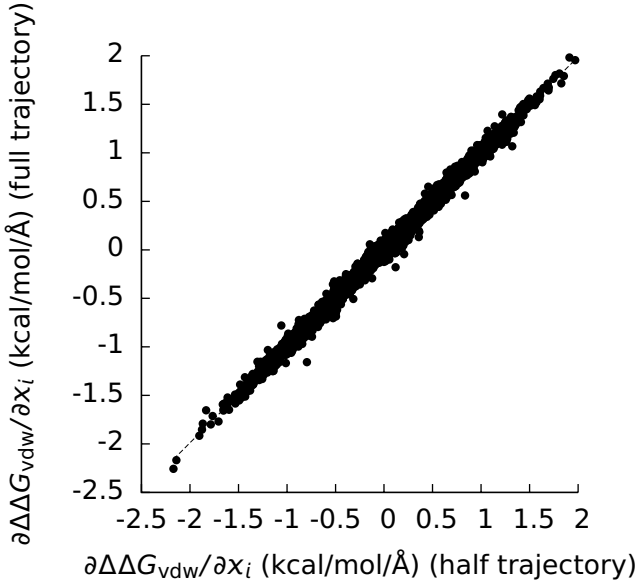
2
1.5
1
0.5
0
-0.5
-1
-1.5
-2
-2.5
-2.5 -2 -1.5 -1 -0.5 0 0.5 1 1.5 2
$\partial\Delta\Delta G_{\mathrm{vdw}}/\partial x_i$ (kcal/mol/Å) (full trajectory)
$\partial\Delta\Delta G_{\mathrm{vdw}}/\partial x_i$ (kcal/mol/Å) (half trajectory)

(d)

Figure 20: a) The derivatives ($\partial \Delta G_{\mathrm{rep}} / \partial x_i$) of the repulsive component (ΔG_{rep}) of the Lennard-Jones cavity insertion free energy (ΔG_{vdw}) with respect to the coordinates (x_i) of the atomic centers versus the same quantity computed from the first halves of the molecular dynamics trajectories for the 9 protein-protein complexes and their components. b) $\partial \Delta G_{\mathrm{vdw}} / \partial x_i$ versus the same quantity computed from the first halves of the molecular dynamics trajectories for the 9 protein-protein complexes and their components. c) The derivatives ($\partial \Delta \Delta G_{\mathrm{rep}} / \partial x_i$) of the repulsive contribution ($\Delta \Delta G_{\mathrm{rep}}$) of the Lennard-Jones contribution ($\Delta \Delta G_{\mathrm{vdw}}$) of the binding free energy with respect to x_i versus the same quantity computed from the first halves of the molecular dynamics trajectories for the 9 protein-protein complexes and their components. d) $\partial \Delta \Delta G_{\mathrm{vdw}} / \partial x_i$ versus the same quantity computed from the first halves of the molecular dynamics trajectories for the 9 protein-protein complexes and their components. The dashed lines are least-squares lines drawn through the data. The slopes (m) and the squares (R^2) of the Pearson correlation coefficients for these lines are: a) $m = 1.00$ and $R^2 = 0.99$, b) $m = 1.00$ and $R^2 = 1.00$, c) $m = 1.00$ and $R^2 = 0.99$, and d) $m = 0.99$ and $R^2 = 0.99$.

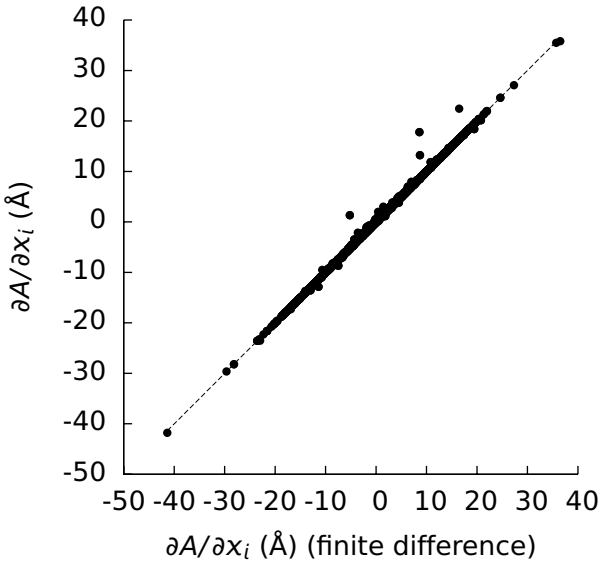

Figure 21: The derivatives ($\partial A / \partial x_i$) of the solvent-accessible surface areas (A) of the protein-protein complexes and their components with respect to the atomic coordinates (x_i) plotted against finite-difference estimates of $\partial A / \partial x_i$ obtained by shifting each atom in each direction by 0.01 Å. The dashed line is a least-squares line drawn through the data. The slope of the line and the square of the Pearson correlation coefficient are 1.00.

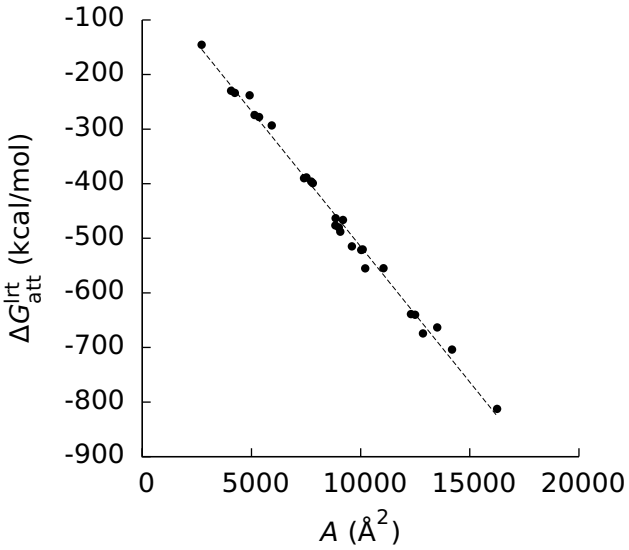

Figure 22: Linear response theory estimates ($\Delta G_{\mathrm{att}}^{\mathrm{lrt}}$) of the attractive component of the free energy required to insert a Lennard-Jones cavity into solution for the nine protein-protein complexes and their components plotted against the solvent-accessible surface area. The dashed line is a least-squares line drawn through the points. Its slope is -0.050 kcal/mol/Å^2, its y-intercept is -19 kcal/mol, and the square of its Pearson's correlation coefficient is 0.992.

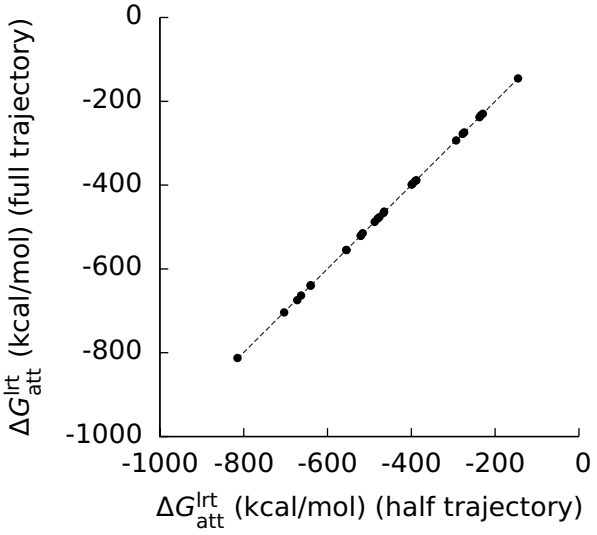

Figure 23: Linear response theory estimates ($\Delta G_{\rm att}^{\rm lrt}$) of the attractive component of the free energy required to insert a Lennard-Jones cavity into solution for the nine protein-protein complexes and their components computed from the full simulation trajectories plotted against $\Delta G_{\rm att}^{\rm lrt}$ computed from the first halves of the simulation trajectories. The dashed line is a least-squares line drawn through the points. Its slope is 0.999, its y-intercept is -0.6 kcal/mol, and the square of its Pearson's correlation coefficient is 0.99997.

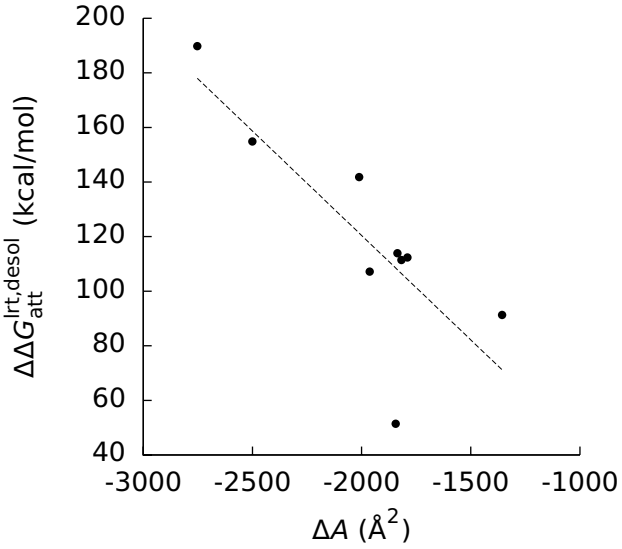

Figure 24: Linear response theory estimates ($\Delta\Delta G_{\rm att}^{\rm lrt}$) of the attractive component of the desolvation free energy for the nine protein-protein complexes plotted against the change (ΔA) in the solvent-accessible surface area upon binding. The dashed line is a least-squares line drawn through the points. Its slope is -0.077 kcal/mol/Å, its y-intercept is -33 kcal/mol, and the square of its Pearson's correlation coefficient is 0.64.

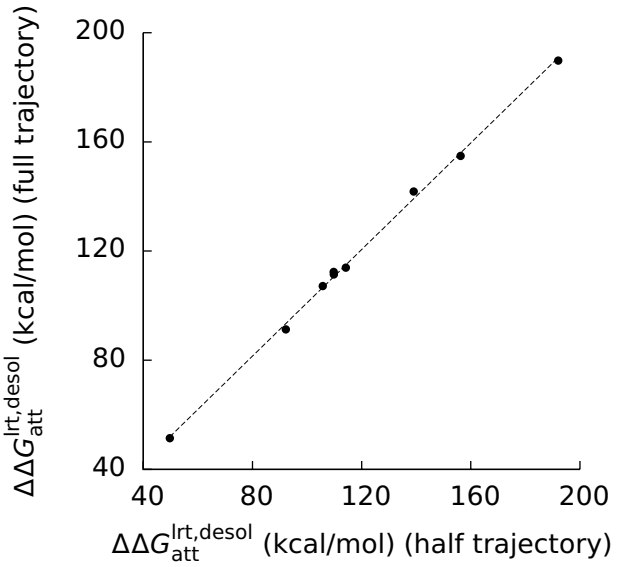

Figure 25: Linear response theory estimates ($\Delta\Delta G_{\rm att}^{\rm lrt,desol}$) of the attractive component of the desolvation free energy for the nine protein-protein complexes computed from the full simulation trajectories plotted against $\Delta\Delta G_{\rm att}^{\rm lrt,desol}$ computed from the first halves of the simulation trajectories. The dashed line is a least-squares line drawn through the points. Its slope is 0.98, its y-intercept is 3.4 kcal/mol, and the square of its Pearson's correlation coefficient is 0.998.

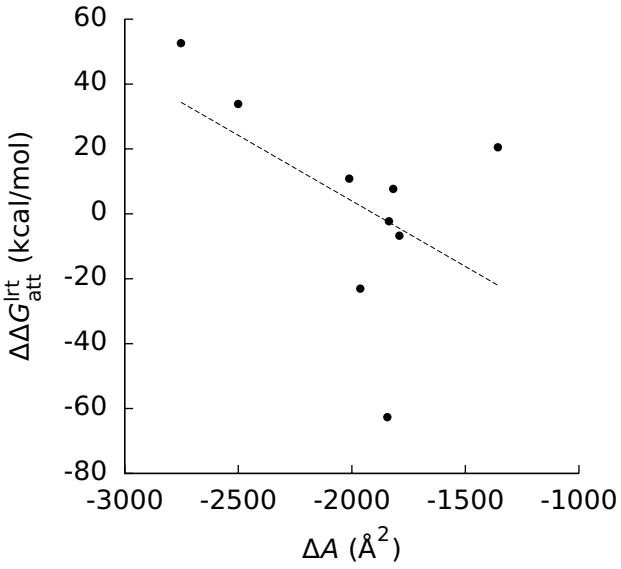

Figure 26: Linear response theory estimates ($\Delta\Delta G_{\rm att}^{\rm lrt}$) of the attractive component of the binding free energy for the nine protein-protein complexes plotted against the change (ΔA) in the solvent-accessible surface area upon binding. The dashed line is a least-squares line drawn through the points. Its slope is -0.040 kcal/mol/Å, its y-intercept is -77 kcal/mol, and the square of its Pearson's correlation coefficient is 0.25.

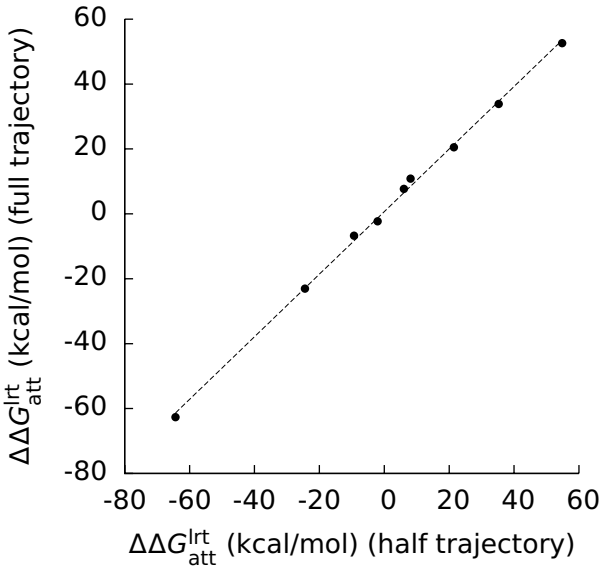

Figure 27: Linear response theory estimates ($\Delta\Delta G^{\mathrm{lrt}}_{\mathrm{att}}$) of the attractive component of the binding free energy for the nine protein-protein complexes computed from the full simulation trajectories plotted against $\Delta\Delta G^{\mathrm{lrt}}_{\mathrm{att}}$ computed from the first halves of the simulation trajectories. The dashed line is a least-squares line drawn through the points. Its slope is 0.96, its y-intercept is 0.69 kcal/mol, and the square of its Pearson's correlation coefficient is 0.998.

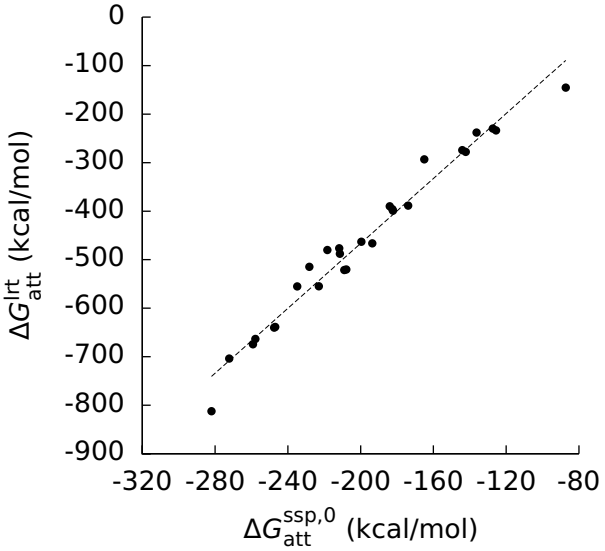

Figure 28: Linear response theory estimates ($\Delta G^{\mathrm{lrt}}_{\mathrm{att}}$) of the attractive component (ΔG_{att}) of the free energy required to insert a Lennard-Jones cavity into solution for the nine protein-protein complexes plotted against estimates ($\Delta G^{\mathrm{ssp,0}}_{\mathrm{att}}$) of ΔG_{att} obtained with single step perturbation using the initial configuration of solvent. The dashed line is a least-squares line drawn through the points. Its slope is 3.4, its y-intercept is 203 kcal/mol, and the square of its Pearson's correlation coefficient is 0.97.

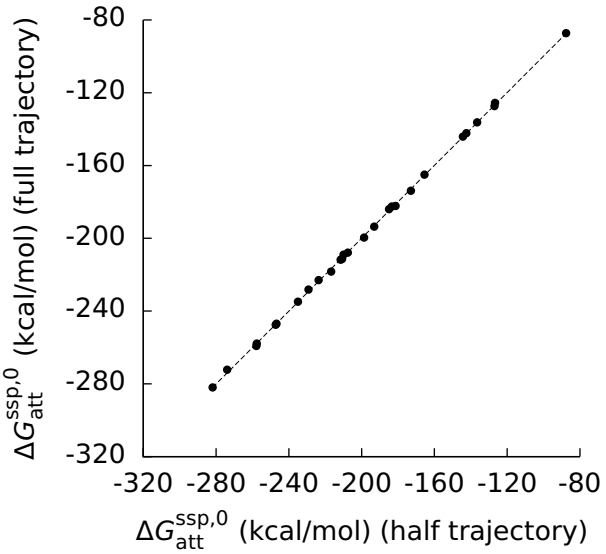

Figure 29: Single step perturbation estimates ($\Delta\Delta G_{\mathrm{att}}^{\mathrm{ssp},0}$) of the attractive component of the binding free energy using the initial configurations of the solvent for the nine protein-protein complexes computed from the full simulation trajectories plotted against $\Delta\Delta G_{\mathrm{att}}^{\mathrm{ssp},0}$ computed from the first halves of the simulation trajectories. The dashed line is a least-squares line drawn through the points. Its slope is 1.001, its y-intercept is 0.30 kcal/mol, and the square of its Pearson's correlation coefficient is 0.997.

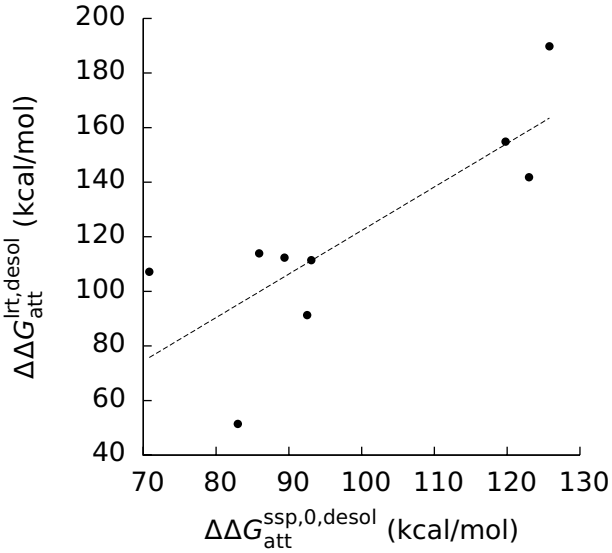

Figure 30: Linear response theory estimates ($\Delta\Delta G_{\rm att}^{\rm lrt,desol}$) of the attractive component ($\Delta\Delta G_{\rm att}^{\rm desol}$) of the desolvation free energy for the nine protein-protein complexes plotted against estimates ($\Delta\Delta G_{\rm att}^{\rm ssp,0}$) of $\Delta\Delta G_{\rm att}^{\rm desol}$ obtained with single step perturbation using the initial configuration of solvent. The dashed line is a least-squares line drawn through the points. Its slope is 1.60, its y-intercept is -37 kcal/mol, and the square of its Pearson's correlation coefficient is 0.64.

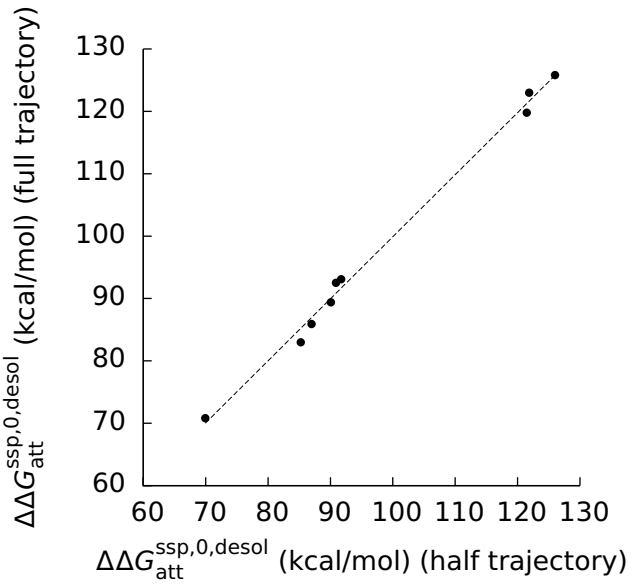

Figure 31: Single step perturbation estimates ($\Delta\Delta G_{\rm att}^{\rm ssp,0}$) of the attractive component of the desolvation free energy using the initial configurations of the solvent for the nine protein-protein complexes computed from the full simulation trajectories plotted against $\Delta\Delta G_{\rm att}^{\rm ssp,0}$ computed from the first halves of the simulation trajectories. The dashed line is a least-squares line drawn through the points. Its slope is 0.995, its y-intercept is 0.43 kcal/mol, and the square of its Pearson's correlation coefficient is 0.995.

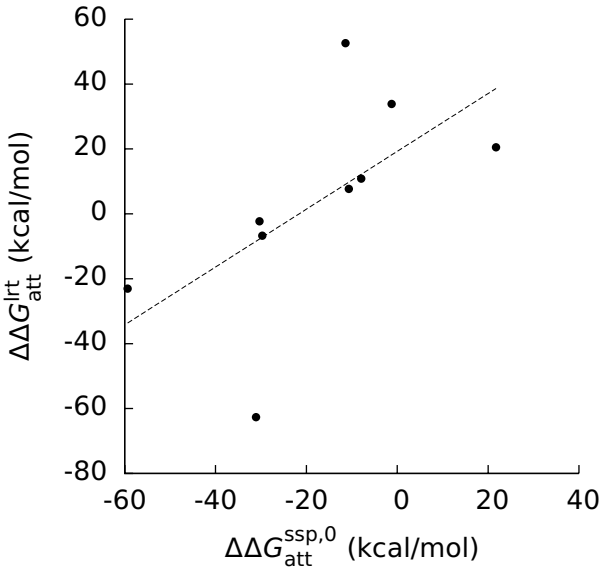

Figure 32: Linear response theory estimates ($\Delta\Delta G_{\rm att}^{\rm lrt}$) of the attractive component ($\Delta\Delta G_{\rm att}$) of the binding free energy for the nine protein-protein complexes plotted against estimates ($\Delta\Delta G_{\rm att}^{\rm ssp,0}$) of $\Delta\Delta G_{\rm att}$ obtained with single step perturbation using the initial configuration of solvent. The dashed line is a least-squares line drawn through the points. Its slope is 0.89, its y-intercept is 19 kcal/mol, and the square of its Pearson's correlation coefficient is 0.38.

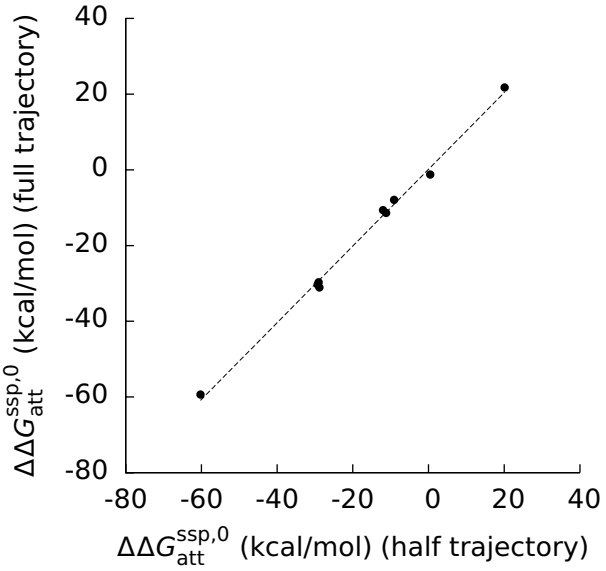

Figure 33: Single step perturbation estimates ($\Delta\Delta G_{\mathrm{att}}^{\mathrm{ssp},0}$) of the attractive component of the binding free energy using the initial configurations of the solvent for the nine protein-protein complexes computed from the full simulation trajectories plotted against $\Delta\Delta G_{\mathrm{att}}^{\mathrm{ssp},0}$ computed from the first halves of the simulation trajectories. The dashed line is a least-squares line drawn through the points. Its slope is 1.01, its y-intercept is 0.14 kcal/mol, and the square of its Pearson's correlation coefficient is 0.996.

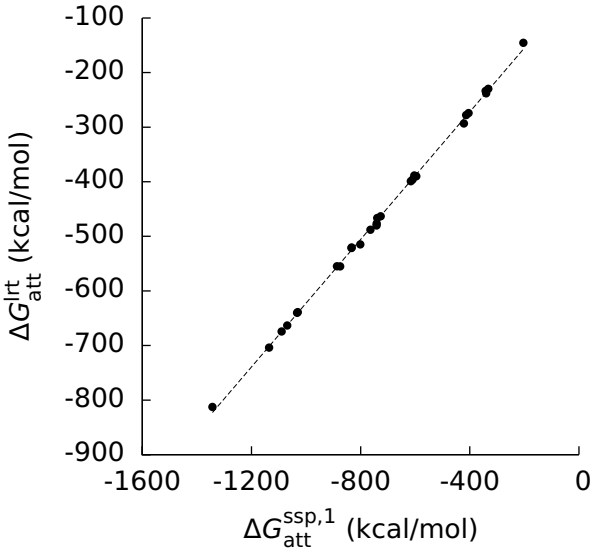

Figure 34: Linear response theory estimates ($\Delta G_{\mathrm{att}}^{\mathrm{lrt}}$) of the attractive component (ΔG_{att}) of the free energy required to insert a Lennard-Jones cavity into solution for the nine protein-protein complexes plotted against estimates ($\Delta G_{\mathrm{att}}^{\mathrm{ssp},1}$) of ΔG_{att} obtained with single step perturbation using the final configuration of solvent. The dashed line is a least-squares line drawn through the points. Its slope is 0.58, its y-intercept is -38 kcal/mol, and the square of its Pearson's correlation coefficient is 0.9991.

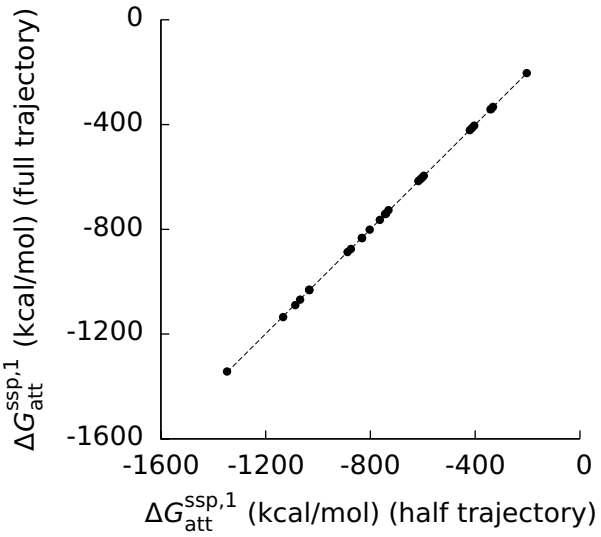

Figure 35: Single step perturbation estimates ($\Delta\Delta G_{att}^{ssp,1}$) of the attractive component of the binding free energy using the final configurations of the solvent for the nine protein-protein complexes computed from the full simulation trajectories plotted against $\Delta\Delta G_{att}^{ssp,1}$ computed from the first halves of the simulation trajectories. The dashed line is a least-squares line drawn through the points. Its slope is 0.998, its y-intercept is -1.25 kcal/mol, and the square of its Pearson's correlation coefficient is 0.99996.

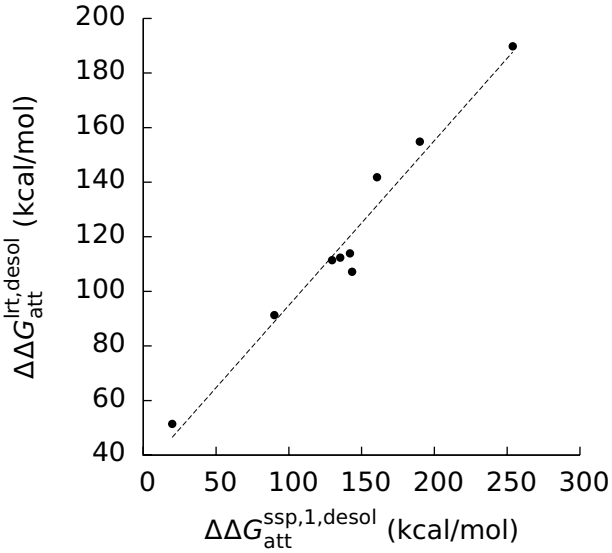

Figure 36: Linear response theory estimates ($\Delta\Delta G_{\mathrm{att}}^{\mathrm{lrt,desol}}$) of the attractive component ($\Delta\Delta G_{\mathrm{att}}^{\mathrm{desol}}$) of the desolvation free energy for the nine protein-protein complexes plotted against estimates ($\Delta\Delta G_{\mathrm{att}}^{\mathrm{ssp},1}$) of $\Delta\Delta G_{\mathrm{att}}^{\mathrm{desol}}$ obtained with single step perturbation using the final configuration of solvent. The dashed line is a least-squares line drawn through the points. Its slope is 0.60, its y-intercept is 35 kcal/mol, and the square of its Pearson's correlation coefficient is 0.97.

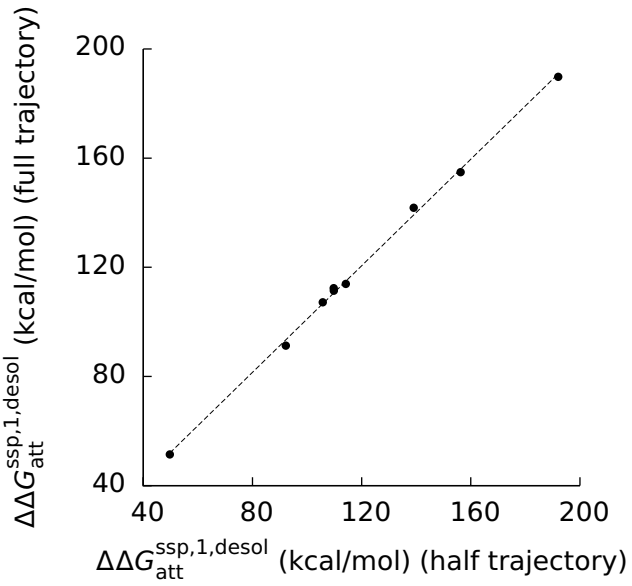

Figure 37: Single step perturbation estimates ($\Delta\Delta G_{\mathrm{att}}^{\mathrm{ssp},1}$) of the attractive component of the desolvation free energy using the final configurations of the solvent for the nine protein-protein complexes computed from the full simulation trajectories plotted against $\Delta\Delta G_{\mathrm{att}}^{\mathrm{ssp},1}$ computed from the first halves of the simulation trajectories. The dashed line is a least-squares line drawn through the points. Its slope is 0.98, its y-intercept is 3.41 kcal/mol, and the square of its Pearson's correlation coefficient is 0.998.

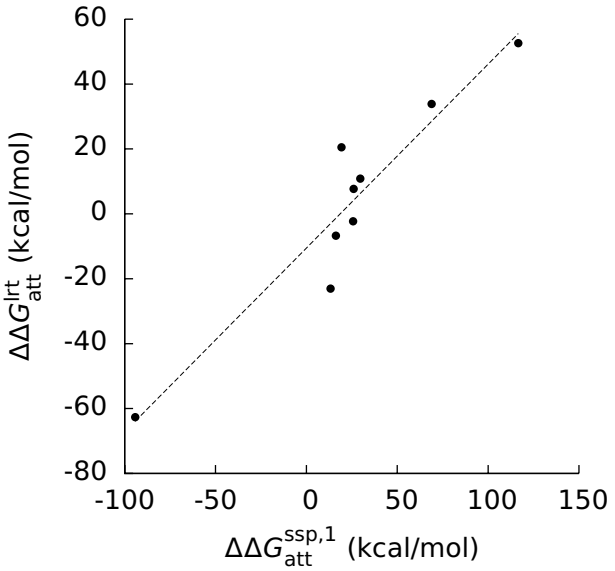

Figure 38: Linear response theory estimates ($\Delta\Delta G_{\rm att}^{\rm lrt}$) of the attractive component ($\Delta\Delta G_{\rm att}$) of the binding free energy for the nine protein-protein complexes plotted against estimates ($\Delta\Delta G_{\rm att}^{\rm ssp,1}$) of $\Delta\Delta G_{\rm att}$ obtained with single step perturbation using the final configurations of solvent. The dashed line is a least-squares line drawn through the points. Its slope is 0.57, its y-intercept is -10.5 kcal/mol, and the square of its Pearson's correlation coefficient is 0.89.

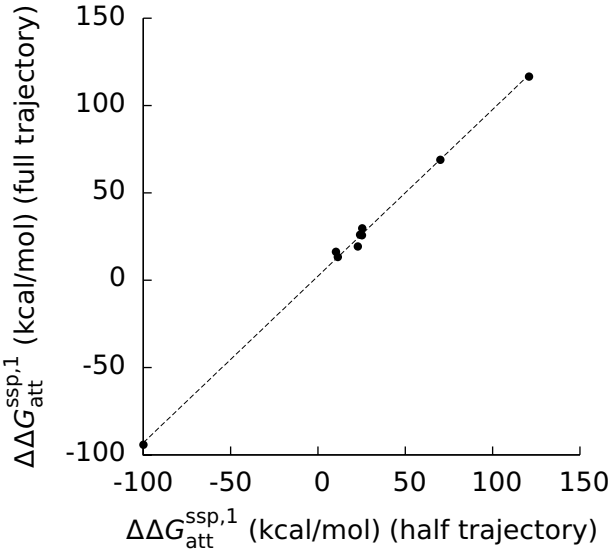

Figure 39: Single step perturbation estimates ($\Delta\Delta G_{\mathrm{att}}^{\mathrm{ssp},1}$) of the attractive component of the binding free energy using the final configurations of the solvent for the nine protein-protein complexes computed from the full simulation trajectories plotted against $\Delta\Delta G_{\mathrm{att}}^{\mathrm{ssp},1}$ computed from the first halves of the simulation trajectories. The dashed line is a least-squares line drawn through the points. Its slope is 0.95, its y-intercept is 2.34 kcal/mol, and the square of its Pearson's correlation coefficient is 0.998.

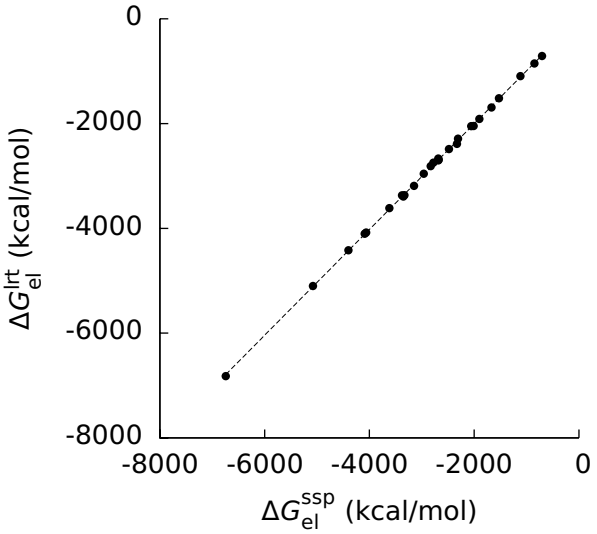

Figure 40: Linear response theory estimates ($\Delta G_{\mathrm{el}}^{\mathrm{lrt}}$) of the electrostatic component (ΔG_{el}) of the solvation free energy for the nine protein-protein complexes and their components plotted against estimates ($\Delta G_{\mathrm{el}}^{\mathrm{ssp}}$) of ΔG_{el} obtained with single step perturbation using the final configuration of solvent. The dashed line is a least-squares line drawn through the points. Its slope is 1.01, its y-intercept is 16 kcal/mol, and the square of its Pearson's correlation coefficient is 0.9997.

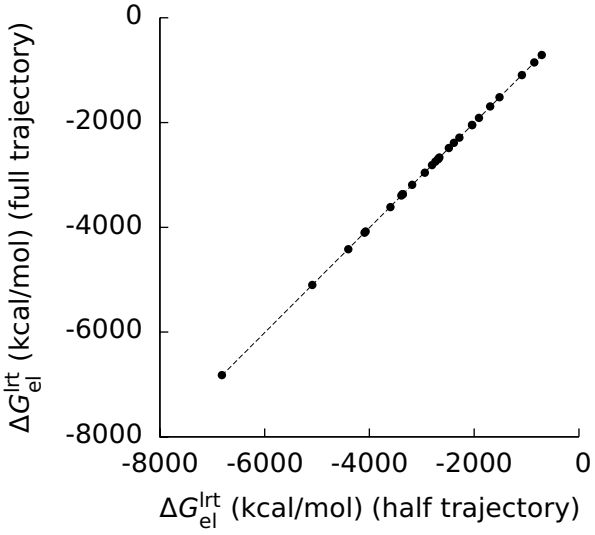

Figure 41: Linear response theory estimates (ΔG_{el}^{lrt}) of the electrostatic component of the solvation free energy for the nine protein-protein complexes and their components computed from the full simulation trajectories plotted against ΔG_{el}^{lrt} computed from the first halves of the simulation trajectories. The dashed line is a least-squares line drawn through the points. Its slope is 1.002, its y-intercept is -0.97 kcal/mol, and the square of its Pearson's correlation coefficient is 0.99999.

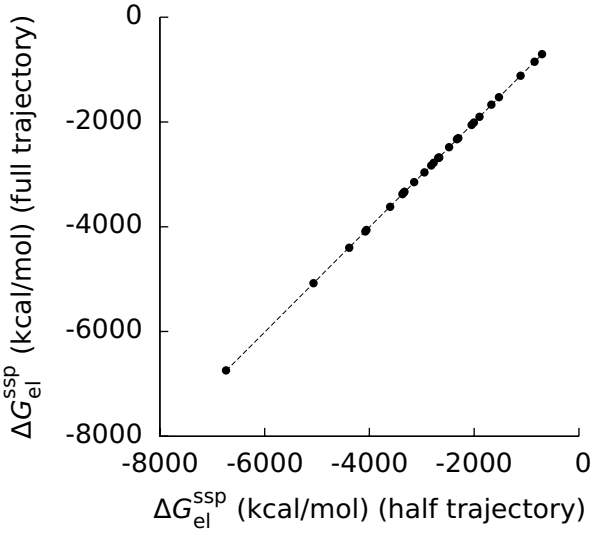

Figure 42: Single step perturbation estimates (ΔG_{el}^{ssp}) of the electrostatic component of the solvation free energy for the nine protein-protein complexes and their components computed from the full simulation trajectories plotted against ΔG_{el}^{ssp} computed from the first halves of the simulation trajectories. The dashed line is a least-squares line drawn through the points. Its slope is 1.002, its y-intercept is -0.17 kcal/mol, and the square of its Pearson's correlation coefficient is 0.99999.

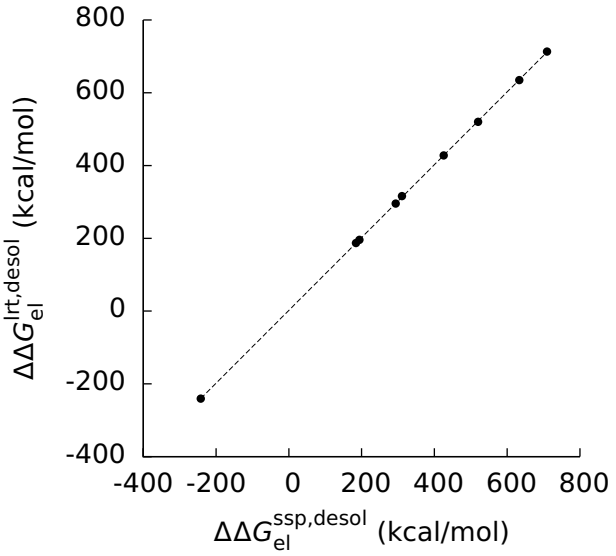

Figure 43: Linear response theory estimates ($\Delta\Delta G_{\rm el}^{\rm lrt,desol}$) of the electrostatic component ($\Delta\Delta G_{\rm el}^{\rm desol}$) of the desolvation free energy for the nine protein-protein complexes plotted against estimates ($\Delta\Delta G_{\rm el}^{\rm ssp,desol}$) of $\Delta\Delta G_{\rm el}^{\rm desol}$ obtained with single step perturbation using the final configuration of solvent. The dashed line is a least-squares line drawn through the points. Its slope is 1.0007, its y-intercept is 2.0 kcal/mol, and the square of its Pearson's correlation coefficient is 0.99997.

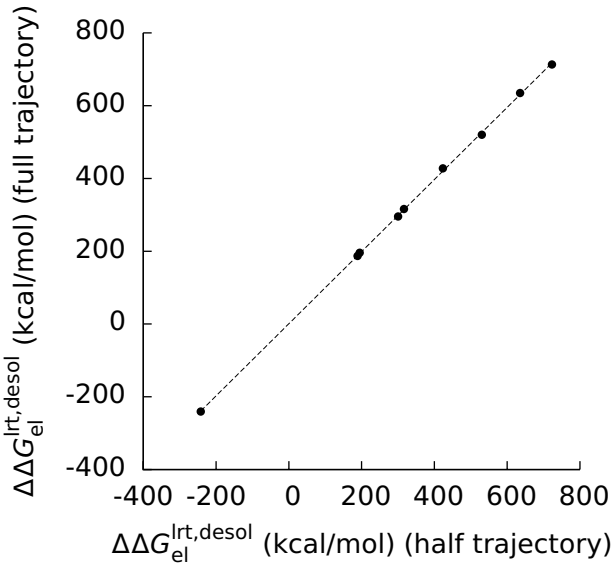

Figure 44: Linear response theory estimates ($\Delta\Delta G_{\mathrm{el}}^{\mathrm{lrt,desol}}$) of the electrostatic component of the desolvation free energy for the nine protein-protein complexes computed from the full simulation trajectories plotted against $\Delta\Delta G_{\mathrm{el}}^{\mathrm{lrt,desol}}$ computed from the first halves of the simulation trajectories. The dashed line is a least-squares line drawn through the points. Its slope is 0.991, its y-intercept is 0.72 kcal/mol, and the square of its Pearson's correlation coefficient is 0.9998.

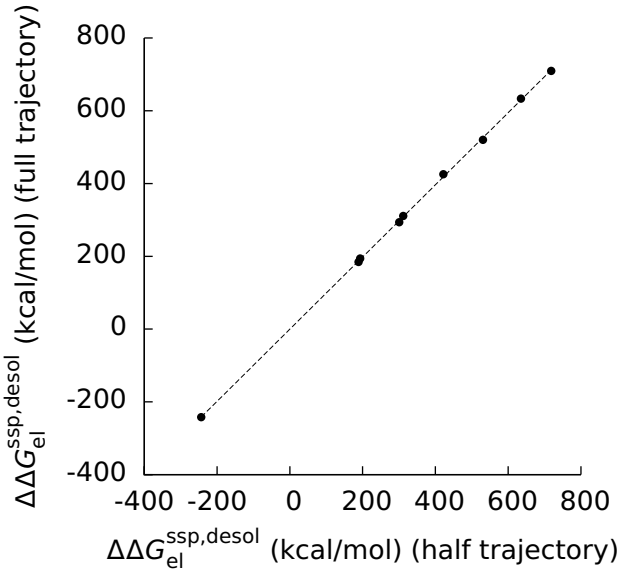

Figure 45: Single step perturbation estimates ($\Delta\Delta G_{\mathrm{el}}^{\mathrm{ssp,desol}}$) of the electrostatic component of the desolvation free energy for the nine protein-protein complexes computed from the full simulation trajectories plotted against $\Delta\Delta G_{\mathrm{el}}^{\mathrm{ssp,desol}}$ computed from the first halves of the simulation trajectories. The dashed line is a least-squares line drawn through the points. Its slope is 0.992, its y-intercept is -0.23 kcal/mol, and the square of its Pearson's correlation coefficient is 0.9998.

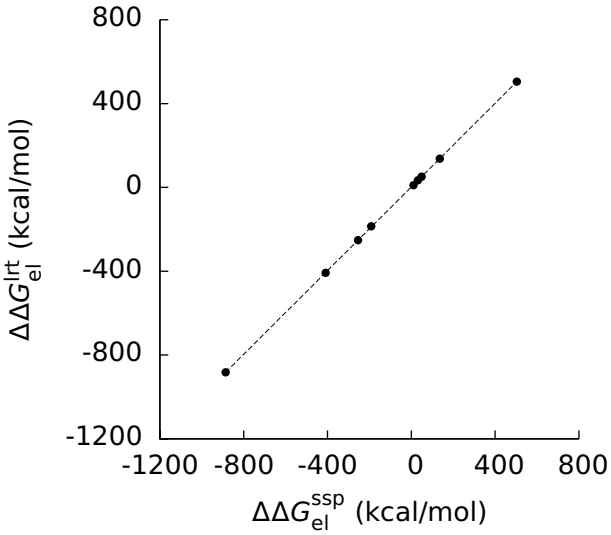

Figure 46: Linear response theory estimates ($\Delta\Delta G_{\rm el}^{\rm lrt}$) of the electrostatic component ($\Delta\Delta G_{\rm el}$) of the binding free energy for the nine protein-protein complexes plotted against estimates ($\Delta\Delta G_{\rm el}^{\rm ssp}$) of $\Delta\Delta G_{\rm el}$ obtained with single step perturbation using the final configuration of solvent. The dashed line is a least-squares line drawn through the points. Its slope is 0.998, its y-intercept is 2.0 kcal/mol, and the square of its Pearson's correlation coefficient is 0.99999.

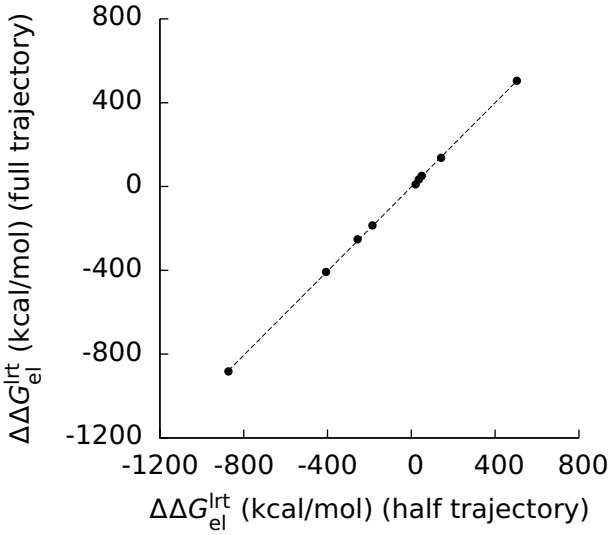

Figure 47: Linear response theory estimates ($\Delta\Delta G_{\rm el}^{\rm lrt}$) of the electrostatic component of the binding free energy for the nine protein-protein complexes computed from the full simulation trajectories plotted against $\Delta\Delta G_{\rm el}^{\rm lrt}$ computed from the first halves of the simulation trajectories. The dashed line is a least-squares line drawn through the points. Its slope is 1.004, its y-intercept is -1.88 kcal/mol, and the square of its Pearson's correlation coefficient is 0.9999.

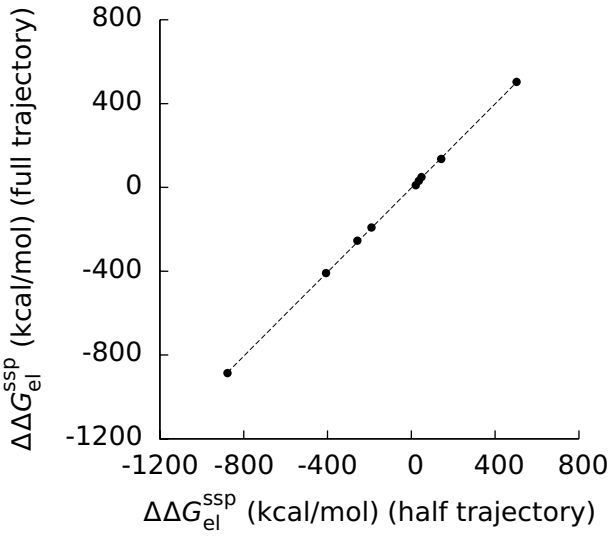

Figure 48: Single step perturbation estimates ($\Delta\Delta G_{\rm el}^{\rm ssp}$) of the electrostatic component of the binding free energy for the nine protein-protein complexes computed from the full simulation trajectories plotted against $\Delta\Delta G_{\rm el}^{\rm ssp}$ computed from the first halves of the simulation trajectories. The dashed line is a least-squares line drawn through the points. Its slope is 1.003, its y-intercept is -2.73 kcal/mol, and the square of its Pearson's correlation coefficient is 0.9999.

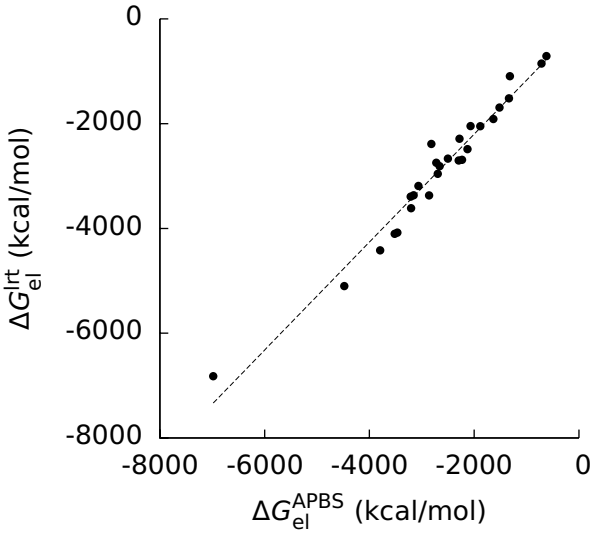

Figure 49: Linear response theory estimates ($\Delta G_{\rm el}^{\rm lrt}$) of the electrostatic component ($\Delta G_{\rm el}$) of the solvation free energy for the nine protein-protein complexes and their components plotted against estimates ($\Delta G_{\rm el}^{\rm APBS}$) of $\Delta G_{\rm el}$ obtained with the Adaptive Poisson-Boltzmann Solver and a mesh spacing of 0.5 Å. The dashed line is a least-squares line drawn through the points. Its slope is 1.03, its y-intercept is -138 kcal/mol, and the square of its Pearson's correlation coefficient is 0.96.

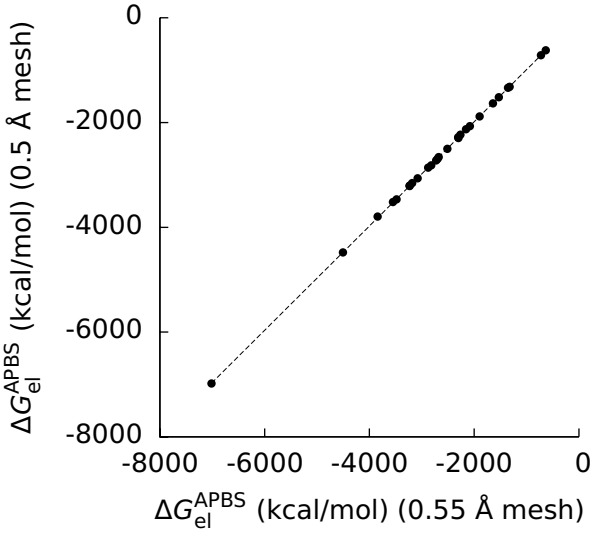

Figure 50: Estimates (ΔG_{el}^{ssp}) of the electrostatic component of the solvation free energy obtained with the Adaptive Poisson-Boltzman Solver (APBS) and a mesh spacing of 0.5 Å for the nine protein-protein complexes and their components plotted against ΔG_{el}^{APBS} computed with a mesh spacing of 0.55 Å. The dashed line is a least-squares line drawn through the points. Its slope is 0.995, its y-intercept is 5.50 kcal/mol, and the square of its Pearson's correlation coefficient is 0.99994.

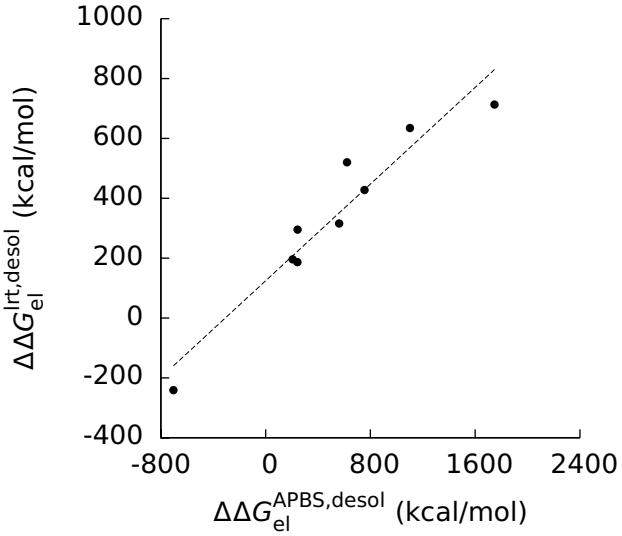

Figure 51: Linear response theory estimates ($\Delta\Delta G_{\mathrm{el}}^{\mathrm{lrt,desol}}$) of the electrostatic component ($\Delta\Delta G_{\mathrm{el}}^{\mathrm{desol}}$) of the desolvation free energy for the nine protein-protein complexes plotted against estimates ($\Delta\Delta G_{\mathrm{el}}^{\mathrm{APBS,desol}}$) of $\Delta\Delta G_{\mathrm{el}}^{\mathrm{desol}}$ obtained with the Adaptive Poisson-Boltzmann Solver and a mesh spacing of 0.5 Å. The dashed line is a least-squares line drawn through the points. Its slope is 0.40, its y-intercept is 125 kcal/mol, and the square of its Pearson's correlation coefficient is 0.92.

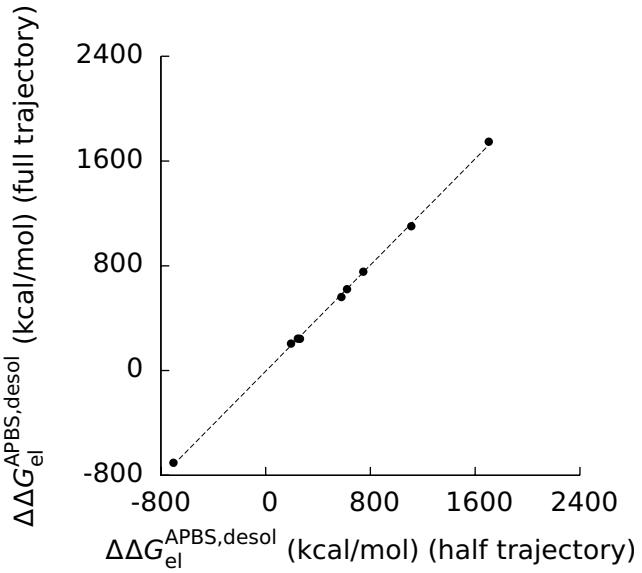

Figure 52: Estimates ($\Delta\Delta G_{\mathrm{el}}^{\mathrm{APBS}}$) of the electrostatic component of the desolvation free energy for the nine protein-protein complexes computed with the Adaptive Poisson-Boltzmann Solver (APBS) and a mesh spacing of 0.5 Å plotted against $\Delta\Delta G_{\mathrm{el}}^{\mathrm{APBS}}$ computed with a mesh spacing of 0.55 Å. The dashed line is a least-squares line drawn through the points. Its slope is 1.01, its y-intercept is -5.36 kcal/mol, and the square of its Pearson's correlation coefficient is 0.9993.

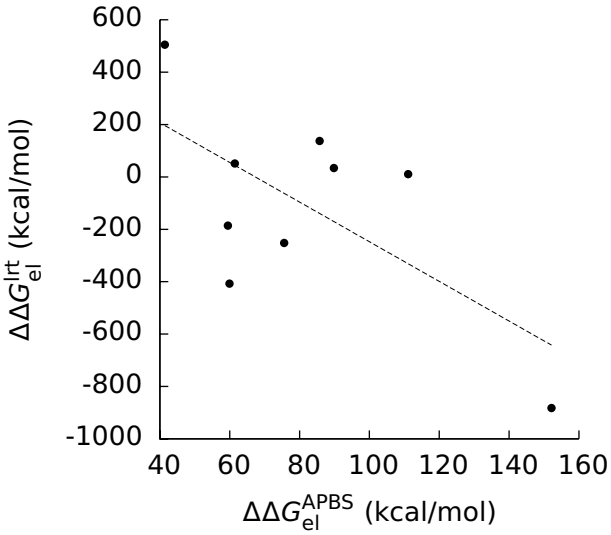

Figure 53: Linear response theory estimates ($\Delta\Delta G_{\rm el}^{\rm lrt}$) of the electrostatic component ($\Delta\Delta G_{\rm el}$) of the binding free energy for the nine protein-protein complexes plotted against estimates ($\Delta\Delta G_{\rm el}^{\rm APBS}$) of $\Delta\Delta G_{\rm el}$ obtained with the Adaptive Poisson-Boltzmann Solver and a mesh spacing of 0.5 Å. The dashed line is a least-squares line drawn through the points. Its slope is -7.57, its y-intercept is 510 kcal/mol, and the square of its Pearson's correlation coefficient is 0.42.

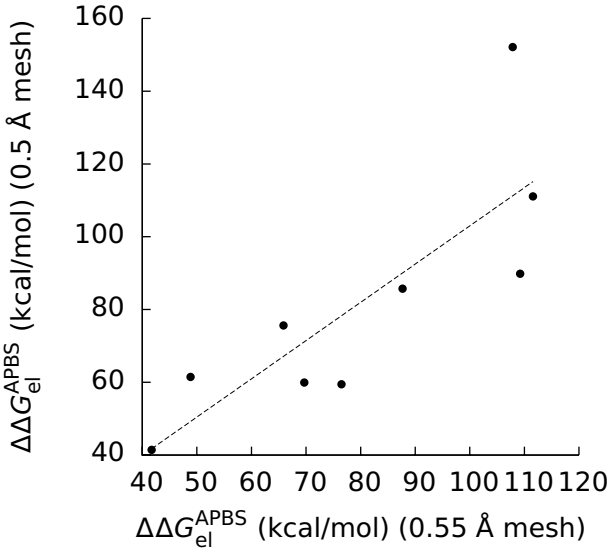

Figure 54: Estimates ($\Delta\Delta G_{\rm el}^{\rm APBS}$) of the electrostatic component of the binding free energy for the nine protein-protein complexes computed with the Adaptive Poisson-Boltzmann Solver (APBS) and a mesh spacing of 0.5 Å plotted against $\Delta\Delta G_{\rm el}^{\rm APBS}$ computed with a mesh spacing of 0.55 Å. The dashed line is a least-squares line drawn through the points. Its slope is 1.05, its y-intercept is -2.09 kcal/mol, and the square of its Pearson's correlation coefficient is 0.67.